SHEAR STRESS CHARACTERISTICS AROUND SLOTTED SPUR-DIKES

A Thesis Submitted
in Partial Fulfilment of the Requirements
for the Degree of
MASTER OF TECHNOLOGY

By
KAUSHAL KUMAR MAURYA

to the

DEPARTMENT OF CIVIL ENGINEERING
INDIAN INSTITUTE OF TECHNOLOGY KANPUR

AUGUST, 1976

CERTIFICATE

This is to certify that the present thesis entitled "Shear Stress Characteristics Around Slotted Spur Dikes" by Kaushal Kumar Maurya (Roll No. 410310), has been carried out under my supervision and results embodied in this thesis have not been submitted elsewhere for award of a degree.

Date: 20th Aug., 1976.

Dr. T. Gangadharaiah
Assistant Professor
Department of Civil Engineering
Indian Institute of Technology
Kanpur.

POST GRADUATE OFFICE
This thesis has been approved for the award of the Degree of Master of Technology (M Tech.) in accordance with the regulations of the Indian Institute of Technology Kanpur
Dated. 31.8.76

ACKNOWLEDGEMENTS

I wish to offer my deep sense of gratitude to Dr. T. Gangadharaiah for his able guidance and sustained encouragement in completing my thesis.

I am also grateful to Dr. K. Subramanya for his valuable suggestions during various stages of the work.

I am also thankful to Mr. S. Kumar for his co-operation needed in setting the experimental set-up. The help rendered during various phases of work by laboratory staff of Hydraulics Lab. is highly appreciated.

I feel pleasure in expressing sense of gratitude to Sri S.D. Dubey, Sri S.D. Misra and Mr. P.D. Porey for creating congenial atmosphere during my work.

Kaushal Kumar Maurya

ABSTRACT

Scour around spurs in river has been a matter of concern to hydraulic engineers from a long time. Scouring phenomenon is essentially governed by shear stress distribution on bed. The present thesis is aimed to elicit the distribution of shear stress near spur on rigid bed.

Shear stress in the channel decreases with increase in opening ratio or decrease in Froude number. The location of maximum shear stress is found to be at $\frac{X}{b} = +1.0$ and $\frac{Z}{b} = +1.8$. The range of relative maximum shear stress i.e. τ_{om}/τ_{ou} is from 5.0 to 1.5 and for tip shear stress τ_{ot}/τ_{ou} is 3.25 to 1.2. Average maximum shear stress occurs at $\frac{X}{b} = .9$ to 1.8, and τ_{oam}/τ_{ou} varies from 4.25 to 1.1.

The difference of water depth in upstream and downstream of spur is more at higher Froude number and lower opening ratio of slotted spur and decreases at lower Froude number and higher opening ratio.

Strouhal number decreases with increase in Froude number or Reynold number. Strouhal number increases with decrease in relative maximum shear stress or shear stress at tip.

It is hoped that this investigation will shed some light on the flow characteristics near spur.

TABLE OF CONTENTS

LIST OF SYMBOLS

a'	width of slots in cm
b'	breadth of spur teeth between two slots in cm
b	breadth of spur in cm
b_1	contracted width of channel in cm
B	width of channel in cm
C	Chezy's constant
d	characteristic length
d_o	outer dia. of dynamic pressure tube of Preston tube
f	frequency of vortices
f_{50}	frequency of vortices exceeding 50% of the observation in frequency distribution curve
F	Froude number $= \frac{V}{\sqrt{gh}}$
h	water depth, in cm
h_o	water depth of the end of bottom of protection
h_x	water depth at x distance from spur in cm
K_1, K_2	constants
p	ratio of maximum shear stress to upstream shear stress $= \tau_{om}/\tau_{ou}$
P_o	static pressure in dyne/cm^2
P_t	total pressure in dyne/cm^2
q	ratio of shear stress at tip of spur to upstream shear stress $= \tau_{ot}/\tau_{ou}$

R	Reynold number $= \frac{V_o d}{\nu}$
R^*	reduced Reynold number $= \frac{V_c d}{\nu}$
S	Strouhal number $= \frac{fd}{V_o}$
S_b	Strouhal number at bottom
S^*	reduced Strouhal number $= \frac{f_1 d}{V_c}$
t	thickness of spur, in cm
u	velocity at y distance from reference plane
V_*	shear velocity $= \sqrt{\tau_o/\rho}$
V_{av}	average velocity in cm/sec
V_c	mean velocity in contracted section, cm/sec
V_R	the resultant velocity in cm/sec
	opening ratio of slotted spur $= \frac{\text{opening area}}{\text{total area}}$
$\varkappa$	constant $= 0.4$
γ	specific gravity of water
ν	Kinematic viscosity of water in cm^2/sec
ω	average vorticity
ω_o	the vorticity at spur's nose
τ_o	shear stress at bottom in $dyne/cm^2$
τ_{ou}	shear stress at upstream initial cross-section, in $dyne/cm^2$
τ_{om}	in dyne/cm maximum shear stress, in $dyne/cm^2$
τ_{oam}	average maximum shear stress in $dyne/cm^2$
τ_{ot}	shear stress at tip of spur in $dyne/cm^2$
τ_{ox}	shear stress at distance x from spur in $dyne/cm^2$

LIST OF FIGURES

CHAPTER 1

INTRODUCTION AND LITERATURE REVIEW

1.1 INTRODUCTION

The problem of scour around a hydraulic structure such as spur-dikes, bridge piers etc. which are placed in alluvial channel is of great importance to the hydraulic engineers. It is important to have clear knowledge on the scour phenomenon occurring around these hydraulic structures for their safe design. The scour phenomenon around a spur dike is found to be governed by the change in local flow characteristics. In order to study the change in local flow characteristics around spur-dikes, an investigation is carried out in the hydraulic laboratory.I.I.T. Kanpur.

Spur-dike is a structure extending from the bank of channel towards the main flow. They are of much practical importance as they may be installed in river to serve following purposes - (i) Training the stream flow, (ii) providing protection to bank from erosion and (iii) to deepen the channel.

Spur may be constructed either perpendicular to bank or at an angle upstream or downstream according to the purpose to be surved. A spur built with an inclination

towards downstream is called 'Attracting Spur', and when it is inclined towards upstream it is called 'Repelling Spur'. The spur perpendicular to flow is called 'Deflecting Spur'.

Spurs may also be classified according to type of construction, viz. solid spurs and slotted spurs or permeable spurs. Permeable spur allows restricted flow through them. Permeable spurs are of very much practical importance as they bear less resistance of water currents compared to solid spur.

Introduction of spur in the channel disturbs the preexisting flow pattern of channel. It obstructs the flow and provides stagnent zone of water pool near junction of spur and bank. Thus spur accelerates the flow in the channel and changes the velocity distribution in the channel which ultimately lead to change the shear stress distribution in channel. The knowledge of shear stress near spur is of much importance as one may be able to predict the scouring pattern in that region.

The literature relating to the hydraulic behaviour of slotted spur-dike is very scant (4) till now considering its practical importance. So, strong need is felt to perform experiments on rigid bed which may explore the characteristics of flow near spur-dike. The present thesis deals with the shear stress distribution on a rigid

bed channel near solid and slotted spurs. Experiments are conducted to study the shear stress pattern for different slotted spurs and solid spur at varying Froude numbers. The aim of project is to determine the bed shear stress contours, maximum shear stress, shear stress at tip and variation of overall shear stress along channel and at different cross-sections for different spur conditions at different Froude number. Vortex shedding measurement is also carried out for solid spur with different Froude number.

1.2 REVIEW OF LITERATURE

Much of literature is available on scour around spur (1,3,5,8,9), but literature pertaining to shear stress distribution is only referred here.

Siezo Awazu (1) conducted the experiment on shear around spur-dike. In first part of his experiment he studied the factors causing scour. He installed two spur dike symmetrically one on each side of a fixed bed channel. He conducted the experiments with varying contraction ratio $(1 - \frac{b}{B})$ from .1 to .4 where b is breadth of spur and 'B' is channel width. The range of Froude number under which experiments were conducted is 0.488 to 0.526. He observed the minimum depth and maximum velocity at centre-line of channel bottom. He related the shear stress to the depth

of flow and bed velocity at centre-line by empirical relation as follows

$$\text{Log}\left(\frac{\tau_{ox}}{\tau_{on\ max}}\right) = 1.40\left(1 - \frac{b}{B}\right) - .021 \qquad (1)$$

where τ_o is shear stress at bottom. Subscript 'n' denotes hydraulic quantities corresponding to the normal flow where a spur-dike is to be installed and 'x' refers to the position of cross-section.

Ippen and Drinker (7) studied the shear stress in curved trapezoidal channel. Boundary shear stress controls the erosion and movement of bed-material in an alluival channel free from obstruction. They attempted to know the shear pattern in curved trapezoidal channel, where effect of local acceleration and secondary motion was also considered in addition to shear stress. They studied that there is a trend of increasing boundary shear stresses with increasing curvature. Shear stress distribution is found to be function of flow condition as well as channel configuration.

McCorquodale and Zaghloul (13) studied a numerical model for flow past a spur-dike. They developed a mathematical model to simulate the scour around a spur-dike. They computed bed shear stresses from the local velocity, turbulence and vorticity as follows.

$$\tau_o = [V_{av}\{1 + f(\omega) + f(\eta)\}]^2 \qquad (2)$$

where V_{av} = average velocity, $f(\omega)$ = vorticity correction and $f(\eta)$ = turbulence correction.

They developed an empirical equation based on above equation as

$$\tau_o = \frac{\gamma}{C^2} V_R^2 \left(1 + K_1 \frac{\omega}{\omega_o} + K_2\right)^2 \qquad (3)$$

where γ = specific weight of water, C = Chezy's coefficient, V_R = the resultant velocity, K_1 and K_2 = constants, ω = average vorticity vector and ω_o = the vorticity at dike's nose.

High velocity and vorticity are found in the region of dike's nose and along the separation line. A trail of vortices travelling downstream in the vicinity of separation line is also noted. These vortices along with local velocity and turbulence were found main source of erosion.

Vinje (12) studied the flow characteristics of vortices in three dimensional local scour. He tried to co-relate the sediment transport to the characteristics of flow i.e. vortices.

Relf and Simmens (12) studied in wind tunnel that the Strouhal number $S = \frac{f \cdot d}{V_o}$ (where f is frequency of

of vortices, d = characteristics length and V_o is initial velocity) is nearly constant for a value of $10^3 < Re = \frac{V_o d}{\nu} < 10^5$ and vortex street will disappear for $Re > 10^5$. Relf concluded that the formation of Karman vortex street depends on the Re, related to the diameter of object and free stream velocity.

According to Vinje (12) effect of Froude number on Strouhal number is significant in open channel flow. Reynold number also influences Strouhal number. Velocity gradient is also an important factor as for as strength of vortices are concerned and are proportional to the Froude number. Vinje (12) proposed following equations for a flat plate perpendicular to wall and to the flow direction in terms of the parameters Fr(< 1), R and S, as

$$S^*_{50} \times \frac{B}{\sqrt{bh_o}} = 2 \times g \times 10^{-3} \, (\bar{R}^*)^{-0.88} \qquad (4)$$

$$S^*_{50} = 0.3 \times g \times \left(\frac{\bar{V}_c}{\sqrt{gh_o}}\right)^{-0.92} \qquad (5)$$

where h_o = water depth at the end of bottom protection, $\bar{V}_c$ = mean velocity in contracted area, S^*_{50} = reduced Strouhal number = $\frac{f}{V_c \, T_{50}}$, $Fr = \frac{V}{\sqrt{gh_o}}$ and Re* = reduced Reynold number = $V_c . d/\nu$, V = mean free stream velocity, ν = kinematic viscosity of water, $\frac{1}{T_{50}}$ = frequency of vortices, exceeding 50% of observations in frequency distribution curve.

CHAPTER 2

EXPERIMENTAL INVESTIGATION

2.1 DETAIL OF EXPERIMENTAL SET-UP

The experiments are conducted in the flume of dimensions 6.0 x 1.0 x .44 meters. Side walls are of glasses and aluminium is on bottom. Valves are provided in the beginning of the flume to adjust discharge and an adjustable gate is at the end to control the depth of flow.

Spurs are made of aluminium. Width of spur is 11 cm (25% of channel width), thickness is 0.6 cm and its height is more than 35 cm. All slotted spurs are having only two slots. Position of spur was kept at a distance of 3.5 m from the adjustable gate at end.

Preston-tube used for measurement of shear stress is same as used by Drinker (7). The details of Preston tube is shown in Figure 2. It consists of two stainless steel tubes whose internal diameters are 0.18" and .09", the outer diameters are 0.25" and 0.125" respectively. The big dia. tube is to be used for dynamic pressure and tube of smaller dia. positioned above at a distance of 0.75" from dynamic tube is used as static pressure tube. Static tube is having two holes of .028" dia. in transverse direction,

The horizontal length of dynamic tube is 1.5" and static tube is .038" more in the same direction. The static tube is positioned above dynamic tube in order to minimize the effect of the total pressure gradient near boundary. The two tubes are welded in upper position and are connected to 15° inclined manometer.

For vortex-shedding measurement, pitot tube was connected to transducer, placed above a plateform near water surface, which in turn was connected to storage type oscilloscope through an amplifier. Details of oscilloscope, Amplifier and Transducer are as follows:

Oscilloscope:

Type: Tektronix manufactured T5640-201 for Type 564 (Mod 8) oscilloscope.

Deflection Plate Sensitivity:- Horizontal: approximately 18.5 volts/cm; Vertical: 19.5 volts/cm.

Screen: 8 cm x 10 cm, deflection and focus is electrostatic one division on horizontal scale measures 5 sec/div. to 1 sec/div. and on vertical scale 10 volt/div. to .01 volt/div.

Amplifier:

Type: 'ENCARDIORITE ELECTRONICS (P) Ltd., India' manufactured "PREAMPLIFIER-PLUG IN ENCARDIORITE MODEL 536".

Sensitivity: .02 mV/cm.

Power Supply for Amplifier: ± 15 V and 200 ma.

Transducer:

Type: 'Temperature compensated pressured transducer "Model No. PG 132 TC-5-350" manufactured by Statham Instruments Inc. 2230, Calif. 13030.

Pressure Range: 0 to 5 psi.

Compensated temperature interval: -65°F to +250°F.

Calibration factor: 1703 microvolts/volts/psi.

2.2 EXPERIMENTAL PROCEDURE

Different discharges were allowed to different depth of flow and so to produce different Froude number. The opening of sluice gate was kept constant throughout the experiment. Two to four shear stress measurements were taken on each side of centre-line of channel across the flow. Along the flow direction, the interval between two measuring cross-sections was 5 cm to 20 cm. Shear stress was measured from 1 m. upstream to 1 m downstream from the

spur position. More closer interval for shear stress measurement was adapted near spur.

The formula used for shear stress calculation from manometer reading is as follows (7).

$$\text{Log}\ \frac{\tau_o\, d_o^2}{4\rho\nu^2} = -1.396 + .875\ \text{Log}\ \frac{(P_t - P_o)d^2}{4\rho\nu^2}$$

$$\text{Valid for range } 4.5 < \text{Log}\ \frac{(P_t - P_e)d^2}{4\rho\nu^2} < 6.5$$

where $(P_t - P_o)$ is the dynamic pressure recorded by a round pitot tube of outer dia 'd_o' and ρ is mass density of fluid. For detail study Appendix may be referred.

In actual measurement, before placing the Preston-tube, maximum velocity direction is established by tuft position. Then Preston tube is placed against the maximum velocity direction and manometer readings are read.

Shear stress in the channel is measured with and without contraction for all five Froude numbers i.e. .475, .338, .258, .209 and .184. Velocity measurements are also taken in centre-line of channel without contraction at spur position.

Water profile is measured by point gauge (having least count .01 cm), for all Froude numbersand spur conditions. Water profile without comtraction is also measuredfor all Froude numbers. Bed profile is measured

to determine the water depth at different sections.

In case of solid spur,wake region is located by placing tuft near water surface for all five Froude number.

In vortex-shedding measurement, water pressure fluctuations are converted in voltage-fluctuation through transducer, which in turn is amplified by amplifier and then fed to oscilloscope. Oscilloscope exhibits these voltage fluctuation on its screen. The horizontal scale measures the movement of fluctuation with time and vertical scale measures its intensity, both can be adjusted by different knobs provided. The signal may be stored upto 24 hrs on its screen. In actual measurement all the signals were stored whenever there were more than two well defined peaks and were traced from the screen. Horizontal and vertical scale readingswere also noted. By horizontal scale reading, one can determine the time interval between two well defined signal peaks i.e. time of vortex-shedding.

Vortex-shedding measurements were taken placing pitot tube at X = + 3b, Z = 1.45b and Y = .91b to 1.8b, for all five Froude number in case of solid spur.

2.3 DETAIL OF EXPERIMENTAL VARIABLES

Following table provides the information regarding the range of experiments conducted.

TABLE 1

Flume Dimension	0.44 x 1.0 x 6.0 meters
Spur dimension	
Solid spur	b = 11.0 cm, t = .6 cm, [illegible] β = 0
15% slotted spur	b = 11.0 cm, t = .6 cm, a' = 0.825 cm, b' = 3.12 cm, β = 15%
25% slotted spur	b = 11.0 cm, t = .6 cm, a' = 1.375 cm, b' = 2.75 cm, β = 25%
33% slotted spur	b = 11.0 cm, t = .6 cm, a' = 1.815 cm, b' = 2.46 cm, β = 33%
Froude number	.475, .338, .258, .209 and .184
Depth of flow	5 cm, 7.5 cm, 10 cm, 12.5 cm and 15 cm
Constriction ratio b/B	Constant = 0.25
Number of slots	Constant = 2

β = opening ratio of slotted spur = $\frac{\text{opening area}}{\text{total area}}$ in Z-section of spur dike,

a' = breadth of slots, b' = breadth of spur teeth between two slots

t = thickness of spur

CHAPTER 3

ANALYSIS

The experimental results are analysed and presented here in order to study the shear stress distribution near spur-dike in open channel flow and its effect on water surface profile and vortex formation.

3.1 DISTRIBUTION OF BED SHEAR STRESS

Contours of equal shear stress are plotted for different Froude number and spur condition in Figures(5 to 9). The intensity of shear stress is less in upstream region of spur-dike and distribution of shear stress is more uniform than downstream. The intensity and non-uniformity decreases as opening ratio 'β' increases. In general, as one proceeds in the direction of flow, shear stress first decreases slightly then increases upto certain distance in downstream of spur and again starts decreasing.

Maximum shear stress occurs in case of solid spur and decreases with decrease in Froude number or increase in opening ratio 'β'. The location of maximum shear stress which is almost fixed for all Froude numbers and spur conditions is at $\frac{X}{b}$ = .5 to 1.0 and $\frac{Z}{b}$ = 1.55.

Shear stress increases due to contraction near spur-dike and then decreases as contraction decreases in downstream direction. In case of solid spur, stagnent zone near spur is more defined and stable, resulting higher contraction than slotted spur. This causes the occurrance of maximum shear stress in case of solid spur.

Contour plots in Figures (5 to 9); show the relative intensity of shear stress with respect to upstream section at $\frac{X}{b} = 0.91$. There are closed contours around maximum shear stress. Enclosing contours are elongated in direction of maximum flow. Steepest contour-gradient is encountered where stream emerges from the most contracted section. The stream of maximum velocity is subjected to take a curved path towards wake region. It accelerates the flow further causing maximum shear stress at the junction of the boundary of curved stream and wake region. Line of maximum shear stress can be seen emerging from the tip of the spur towards maximum flow direction.

Distribution of relative shear stress across channel may be viewed in Figures (12 to 14) for Froude numbers .475, .258 and .184 with different spur conditions. The cross-sections taken for study are located at $\frac{X}{b} = -1$, $-\frac{1}{2}$, 0, $+\frac{1}{2}$, +1, +2, +3 and +4. Maximum shear stress occurs near tip and then reduces in lateral direction. In solid

spur case, there is steep fall of shear stress due to well defined and stable wake region near spur. Beside steep fall, a well defined kink in relative shear stress curve is also seen (Figure 12, 13). Kink may be due to separation of two streams passing through contraction. This kink also shifts towards spur as one proceeds towards down stream. These curves also show that in upstream of spur the difference in shear stress of solid and slotted spur is very less but after crossing the contracted section at spur, the difference is quite high. At lower Froude number the difference of shear stress between solid and slotted diminishes.

3.2 AVERAGE BED SHEAR STRESS ALONG CHANNEL

Average shear stress across the channel is calculated excluding wake region. These are plotted along the channel length for different Froude numbers and spur conditions in Figures (10, 11).

Average shear stress first decreases, attains a minimum value ($\frac{\tau_{ox}}{\tau_{ou}}$ = 0.8 to 0.9), then gradually increases acquires maximum near $\frac{X}{b}$ = 1.0 to 1.8 and again decreases. Location of average maximum shear stress shifts towards spur as Froude number reduces for solid spur and same trend is observed as opening ratio β increases at higher Froude number. The difference between relative average shear

stress of different spurs at any section in downstream is more than upstream at higher Froude number. Same trend is observed for different Froude number at lower opening ratio. The apex of the average shear stress curve becomes much flatter and more symmetrical as Froude number reduces. Average shear stress decreases as Froude number decreases or opening ratio of slotted spur increases.

Slight decrease in average shear stress in upstream direction of spur is attributed to the fact that afflux due to obstruction, increases water depth, consequently shear stress reduces. As one proceeds towards spur, due to contraction water is accelerated, so velocity increases, causing shear stress to increase drastically near spur. Though heading up of water just near to spur causes to reduce shear stress, but its effect is very little compared to the effect of contraction. In downstream region of the spur, the portion of stream, near the spur passes in a curved path around spur, leaving other portion of stream to go straight. Curved stream adds more acceleration to accelerated flow producing maximum shear stress. Shear stress is increased further in curved path, since water profile becomes inclined towards centre of curve, so water depth is least for inner most stream of curved stream. Shear stress goes on increasing in direction of flow upto $\frac{X}{b} = 1.8$, and then

decreases due to reduction in velocity in downstream direction as wake region reduces in same direction. Average shear stress also reduces as Froude number reduces because velocity decreases as Froude number decreases. Average shear stress also reduces as opening ratio increases, because of reduction in wake area due to flow through slots. Number of slots providing same opening ratio, also affect the degree of contraction. There should be a limit of $\frac{a'}{b'}$ to give most effective contraction of flow by slotted spur. If one increases $\frac{a'}{b'}$ further, slotted spur may behave like perforated spur.

At lower Froude number average shear stress curves try to become equal for different spur conditions. Same trend can also be visualised at greater opening ratio of slotted spur for different Froude number.

3.3 LOCAL MAXIMUM SHEAR STRESS

The relative local maximum shear stress observed in the present experiments is in case of solid spur at highest Froude number. $\frac{\tau_{om}}{\tau_{ou}}$ is found to be as high as 5.0 in this case. It decreases as Froude number decreases or opening ratio of slotted spur increases keeping other conditions identical. The lowest value of $\frac{\tau_{om}}{\tau_{ou}}$ is around 1.5 in case of slotted spurs at lower Froude number. The

location of maximum shear stress occurs at $\frac{X}{b} = 1.0$ and $\frac{Z}{b} = 1.8$ for all cases with different Froude number and spur condition. The most constracted section of the flow is not at spur position but a little away in downstream of spur, where maximum shear stress occurs. The variation of $\frac{\tau_{om}}{\tau_{ou}}$ is plotted against Froude number taking opening ratio of slotted spur as parameter and is shown in Figure (15). They show a straight line relationship for different spur condition. The gradient of line representing $(\frac{\tau_{om}}{\tau_{ou}} / F)$ generally decreases as opening ratio 'β' of slotted spur increases. Following equations of straight lines relates Froude number with $\frac{\tau_{om}}{\tau_{ou}}$.

$p = .58\ F$ (for solid spur)

$p = .2\ F + .85$ (for 15% slotted spur)

$p = .104\ F + 1.45$ (for 25% slotted spur)

$p = .125\ F + .85$ (for 33% slotted spur)

where $p = \tau_{om}/\tau_{ou}$.

3.4 SHEAR STRESS AT TIP OF SPUR

Relative shear stress at tip i.e. $\frac{\tau_{ot}}{\tau_{ou}}$ essentially follows the same trend as local maximum shear stress as shown in Figure (16). It decreases as Froude number

decreases or opening ratio of slotted spur increases if other conditions are kept constant. The maximum shear stress at tip occurs in case of solid spur having $\frac{\tau_{ot}}{\tau_{ou}} = 3.25$ in case of solid spur when F = 0.475. The lowest value of $\frac{\tau_{ot}}{\tau_{ou}} = 1.2$, occurs at F = 0.184 when $\beta = 33\%$. The values of τ_{ot}/τ_{ou} are found to be proportional to Froude number and can be represented by following straight line equations

$q = .206\ F + 0.5$ (for solid spur)

$q = .133\ F + 1.0$ (for 15% slotted spur)

$q = .057\ F + 1.25$ (for 25% slotted spur)

$q = .08\ F + 1.80$ (for 33% slotted spur)

where $q = \frac{\tau_{ot}}{\tau_{ou}}$.

3.5 WATER SURFACE PROFILE

Average water surface profile goes on rising before spur and then decreases after spur in downstream as shown in Figure (17). Difference in water depth in upstream and downstream is more conspicuous at higher Froude number for all spur conditions. This difference in water depth decreases as Froude number decreases. Water depth decreases before spur in direction of flow and increases after spur with increase in opening ratio of slotted spur

for all Froude numbers. Difference between water depth for different opening ratio of spur for a particular Froude number is more in upstream than downstream of the spur.

Near spur water surface profile is inclined towards spur and behaves as open channel flow passes in a curved path. This inclined water surface has got minimum depth near spur and depth increases in transverse direction at a short distance away from the spur and then decreases in transverse direction. A local depression is also seen in vicinity of the edge of spur. The slope of water surface towards spur decreases as opening ratio of slotted spur increases.

One can also calculate the average shear stress by knowing wake region and water depth. The velocity distribution in open channel is governed by following formula.

$$\frac{u}{V_*} = \frac{1}{\kappa} \ln y \frac{V_*}{\nu} + 5.5 \quad \text{(for smooth turbulent flow)}$$

where u is velocity at depth y, κ = constant = 0.4 and V_* = shear velocity = $\sqrt{\frac{\tau_o}{\rho}}$.

Taking average velocity over depth 'h'

$$\frac{1}{h}\int_{\varepsilon}^{h} \frac{u}{V_*}\, dy = \frac{1}{h}\int_{\varepsilon}^{h} \left(\frac{1}{\kappa} \ln y \frac{V_*}{\nu} + 5.5\right) dy$$

or,

$$\frac{\bar{u}}{V_*} = 5.75 \log \frac{h V_*}{\nu} + 3.0 \qquad (6)$$

$$\bar{u} = V_* \left(5.75 \log_{10} \frac{h V_*}{\nu} + 3.0\right)$$

where $\bar{u}$ is average velocity, considering two cross-sections in channel

$$Q = h_1 b_1 V_* \left(5.75 \log \frac{h_1 V_{*1}}{\nu} + 3.0\right)$$

$$= h_x b_x V_{*x} \left(5.75 \log \frac{h_x V_{*x}}{\nu} + 3.0\right)$$

where suffix 1 and x refers to the initial section and section at x distance, and b is contracted breadth and h is water depth.

$$\frac{\sqrt{\frac{\tau_{o1}}{\rho}}}{\sqrt{\frac{\tau_{ox}}{\rho}}} = \frac{V_{*1}}{V_{*x}} = \frac{h_x b_x}{h_1 b_1} \frac{\left(5.75 \log \frac{h_x b_x}{\nu} + 3.0\right)}{\left(5.75 \log \frac{h_1 b_1}{\nu} + 3.0\right)}$$

$$\text{or,} \quad \frac{\tau_{o1}}{\tau_{ox}} = \left(\frac{h_x b_x}{h_1 b_1}\right)^2 \left\{\frac{\left(5.75 \log \frac{h_x V_{*x}}{\nu} + 3.0\right)}{\left(5.75 \log \frac{h_1 V_{*1}}{\nu} + 3.0\right)}\right\}^2 \qquad (7)$$

For all practical purposes, one can use following formula,

$$\frac{\tau_{ox}}{\tau_{o1}} = \left(\frac{h_1 b_1}{h_x b_x}\right)^2 \qquad (8)$$

The above two equations are plotted in Figure (18). This figure reveals the fact that second term of right hand side in equation (7) has little effect in computation of relative shear stress.

The above analysis is done for all five Froude numbers in case of solid spur and is shown in Figure (19). The accuracy of computation of relative shear stress depends on the actual judgement of wake region, which is difficult to measure precisely. Computed points are scattered around actual relative shear stress curve. The deviation of observed shear stress than computed by equation (8) may be explained on following reasons.

(1) Growth of boundary layer is not considered.

(2) The whole fluid is considered as fully developed turbulent flow.

(3) The flow in equation (7) is considered as uniform flow which is not in practice.

3.6 VORTEX-SHEDDING MEASUREMENTS

Strouhal number ($S = \frac{fd}{V_o}$) is determined for all five Froude numbers in case of solid spur. Strouhal number is taken at fixed location X = +3b, Z = +1.55b, Y = bottom to the water surface. Strouhal number decreases with increase in Froude number as shown in Figure (21).

This curve resembles with Vinje's curve (12). The range of Strouhal number at one Froude number with respect to different vertical position decreases rapidly at higher Froude number.

The relationship between Reynold number and Strouhal number is also displayed in Figure (20). Here also the curve follows the same trend as in case of Froude number. Strouhalnnumber decreases as Reynold number increases.

The effect of Strouhal number on relative maximum shear stress and relative tip shear stress is also studied. For this purpose only bottom Strouhal number is considered. The relationship between bottom Strouhal number and $\frac{\tau_{om}}{\tau_{ou}}$ and $\frac{\tau_{ot}}{\tau_{ou}}$ is shown in Figure (22). Strouhal number decreases as $\frac{\tau_{om}}{\tau_{ou}}$ or $\frac{\tau_{ot}}{\tau_{ou}}$ increases.

CHAPTER 4

CONCLUSION AND RECOMMENDATIONS

4.1 CONCLUSION

Present investigation is aimed to study the shear stress distribution near solid and slotted spurs. Following conclusions are derived from the present work.

1. Study of bed shear reveals the fact that shear stress is non-uniform and more intense near spur. This non-uniformity and intensity of shear stress decreases as opening ratio of slotted spur increases.
2. Shear stress decreases with increase in opening ratio or decrease in Froude number. This trend is true for average shear stress, maximum shear stress and shear stress at tip of spur.
3. Location of maximum shear stress is at $\frac{X}{b} = +1.0$, and $\frac{Z}{b} = +1.8$ for all combination of F and β of slotted spur. The range of $\frac{\tau_{om}}{\tau_{ou}}$ is 5.0 to 1.5 and $\frac{\tau_{ot}}{\tau_{ou}}$ is 3.25 to 1.2. Average maximum shear stress occurs at $\frac{X}{b} =$ +0.9 to +1.8 and $\frac{\tau_{oam}}{\tau_{ou}}$ varies from 4.25 to 1.1. Line of maximum shear starts from tip of spur and follows the direction of maximum flow.

4. Difference of water depth in upstream and downstream of spur is more at higher Froude number and at lower opening ratio of slotted spur and decreases at lower Froude number and higher opening ratio.
5. Strouhal number decreases with increase in Froude number or Reynold number and also accompanied with increase in $\frac{\tau_{om}}{\tau_{ou}}$ or $\frac{\tau_{ot}}{\tau_{ou}}$.

4.2 RECOMMENDATIONS

Further investigation may be done as an extension of present study as follows.

1. Variation of constriction ratio.
2. Variation of opening ratio as well as number of slots.
3. Variation of angle of spur with respect to flow in channel.
4. Extension of limit of Froude number.
5. Strouhal number study for slotted spur.

REFERENCES

1. Awazu, Seizo, (1967). 'On scour around spur dike'. Proceedings of 12th Congress of International Association for hydraulic Research, Vol. 3, Colorado State Univ., Fort Collins, Colorado, U.S.A.
2. Bryer, D.W. and Pankhwst, R.C. (1967). 'Pressure Probe methods for determining wind speed and flow direction'. National Physical Laboratory, Department of Trade and Industry, London.
3. Garde, R.J., Subramanya, K., and Numbudripad, K.D. (1961). 'Study of scour around spur dike'. Journal of Hydraulic Div. ASCE No. HY6, Nov. 1961.
4. Gole, C.V., Chitale, S.V. and Kulkarni, "Slotted Spur". Proc. of Forty Fourth Annual Research Session, Chandigarh, CBI & P Publ. No. 123, Vol. 1, 1975.
5. Hedmann, Rober E. (1965), 'Effect of spur dikes on flow through contraction'. Journal of Hydraulic Div. A.S.C.E., No. HY4, July 1965.
6. Hwang,Li San and Laursen Emmett M. (1963). 'Shear measurement technique for rough surfaces'. Journal of Hydraulic Division, A.S.C.E., No. HY2, March 1963.
7. Ippen, Arther L. and Drinker, Philip A. (1962). 'Boundary shear stresses in curved trapezoidal channel'. Journal of Hydraulic Division A.S.C.E., No. HY5, September 1962.

8. Laursen, Emmet M. (1960). 'Scour at bridge crossing'. Journal of Hydraulic Division, A.S.C.E. No. HY2, Feb. 1960.

9. Laursen, Emmet M. (1963). 'Analysis of relief bridge scour'. Journal of Hydraulic Division, A.S.C.E., No. HY2, May 1963.

10. Preston, J.H. (1953). 'The determination of turbulent skin friction by means of pitot tubes'. Cambridge University Aeronautic Laboratory.

11. Ramamurthy, A.S., Lee, P.M. and Ng, C.P. (1974). 'Blockage effect for single rows of bluff bodies'. Fifth Australian Conference on Hydraulics and Fluid Mechanics at Canterbury Christchurch, Newzealand.

12. Vinje, J.J. (1967). 'On the flow characteristics of vortices in three dimensional local scour'. Proceedings of 12th Congress of I.A.H.S., Vol. 3, Colorado State Univ., Fort Collins, Colorado, U.S.A.

13. Zaghloul, N. and McCorquodale, John A. 'A numerical model for flow past a spur dike'. Dept. of Civil Engineering, University of Windsor, Ontario, N9B 3P4.

APPENDIX

MEASUREMENT OF SHEAR STRESS

The direct measurement of shear stress at boundary has not been of much success. In this method a small isolated floating element is kept at small distance from boundary and shear force acting on it was measured (10). This direct technique involves a lot of precautions so it is impracticable.

A standard indirect method in boundary layer studies involves measurement of the velocity and pressure profile normal to the boundary at different section and solving for shear by momentum principle.

Ludweigh (10) discovered an indirect method for shear measurement. He related shear force to the heat loss from a hot spot on the boundary to flow medium. This method is useful only for laminar sublayer.

In 1954, Preston (10) used Pitot tube for measurement of shear stress. He assumed near the surface where shear stress is to be measured, conditions are functions of skin friction; physical constant of fluid like viscosity and specific gravity; and a suitable length viz., inside dia. of tube, size of roughness. He developed

a non-dimensional relationship for the difference between the total pressure recorded by the tube and the static pressure at wall in terms of skin friction. Near the surface within limits of experimental accuracy, Ludwiegh and Tellmann (10) established following relation,

$$\frac{u}{V_*} = f\left(y \frac{V_*}{\nu}\right) \qquad (9)$$

In which u is the velocity at a distance y from the surface and V_* is the friction velocity. $V_* = \sqrt{\tau_o/\rho}$, where τ_o is skin friction stress. The above result is unaffected by pressure gradient and of upstream disturbances. This region involved is of order of 1/10 of the boundary layer thickness and is therefore many times the thickness of the viscous sublayer. Velocity distributions close to the wall, in viscous sublayer is

$$\frac{u}{V_*} = \frac{V_* y}{\nu} \qquad (10)$$

Ludweigh and Tillmann observed following relation suited for pipes and channels,

$$\frac{u}{V_*} = 5.5 \log_{10} \frac{V_* y}{\nu} + 5.8 \qquad (11)$$

Considering the eqn. (9) which is applicable in a limited region near the wall. So, it must imply a restricted dynamical similarity in this region, for which τ_o, ρ, ν

and some representative length are the only variable. Considering total pressure P as read by one of a set of geometrically similar circular pitot tubes resting on the surface, measured relative to the static pressure p_o at the wall. Then $(P - p_o)$ is the dependent variable depending only on independent variables ρ, ν, τ_o and d. This leads to the following relationship

$$\frac{(P - p_o)\, d^2}{\rho \nu^2} = f\left(\frac{\tau_o\, d^2}{\rho \nu^2}\right) \qquad (12)$$

To determine 'f' we conduct the experiment in a circular pipe or channel where τ_o is calculable from pressure drop. For a circular pipe of internal diameter D

$$\tau_o = (p_1 - p_2)\, \frac{D}{4L} \qquad (13)$$

where $(p_1 - p_2)$ is the pressure drop over a length L. In the above experiment one should take care that pitot must lie entirely in the region where eqns. (9) and (12) holds good and pitot diameter should be small. They conducted several experiments with a set of geometrically similar pitots over a range of $(p_1 - p_2)$. They plot the curve τ_o versus $(P - p_o)$ to determine 'f'. If each pitot tube produces same value of τ_o or

$$C_f = \frac{\tau_o}{\frac{1}{2}\rho V^2} \qquad (14)$$

then it is evidence of the existance of a local dynamical similarity. Equation (12) is equally applicable for pitot tube other shapes than circular. Considering local dynamic similarity one may also write following equation similar as eqn. (12)

$$\frac{(P - p_o)}{\rho V^2} = \phi\left(\frac{\tau_o y^2}{\rho V^2}\right) \qquad (15)$$

where p is static pressure recorded at height y. One may determine ϕ by pipe experiment. τ_o can be checked by eqn. (12) also. Eqn. (15) can be written more precisely, as

$$\left(\frac{(P - p_o)}{\rho V^2} y^2\right) = \phi\left(\frac{\tau_o y^2}{\rho V^2}, \frac{y}{h_p}\right)$$

where h_p is the width of pitot tube. The displacement of the effective centre of the flat pitot was taken to be .25 of the width h_p.

TABLE A1. List of Experimental Variables

β	h (cm)	U (cm/sec)	F	R ($\times 10^4$)	τ_{ou} (dyne/cm^2)	$\frac{\tau_{om}}{\tau_{ou}}$	$\frac{\tau_{ot}}{\tau_{ou}}$	$\frac{\tau_{oam}}{\tau_{ou}}$	S_b
0%	5.0	33.1	.475	4.42	2.60	5.00	3.25	4.25	0.55
	7.5	29.3	.338	3.92	2.30	3.42	2.42	3.00	0.515
	10.0	25.5	.258	3.42	2.30	2.66	1.94	1.90	0.685
	12.5	23.1	.209	3.10	2.10	1.96	1.73	1.60	1.87
	15.0	22.2	.184	2.98	2.00	1.81	1.55	1.50	1.72
15%	5.0	33.1	.475	4.42	2.90	3.26	2.35	2.60	
	7.5	29.3	.338	3.92	3.82	2.16	1.90	1.85	
	10.0	25.5	.258	3.42	3.38	2.22	1.70	1.70	
	12.5	23.1	.209	3.10	1.72	2.00	1.60	1.48	
	15.0	22.1	.184	2.98	1.59	1.90	1.55	1.50	
25%	5.0	33.1	.475	4.42	5.10	2.42	1.40	1.95	
	7.5	29.3	.338	3.92	3.50	2.24	1.66	1.90	
	10.0	25.5	.258	3.42	3.00	2.32	1.55	1.80	
	12.5	23.1	.209	3.10	2.70	1.89	1.56	1.65	
	15.0	22.2	.184	2.98	2.30	1.75	1.53	1.20	
33%	5.0	33.1	.475	4.42	4.90	2.22	1.70	1.50	
	7.5	29.3	.338	3.92	3.10	1.80	1.56	1.45	
	10.0	25.5	.258	3.42	2.50	2.10	1.47	1.70	
	12.5	23.1	.209	3.10	2.40	1.44	1.30	1.05	
	15.0	22.2	.184	2.98	2.30	1.35	1.18	1.05	

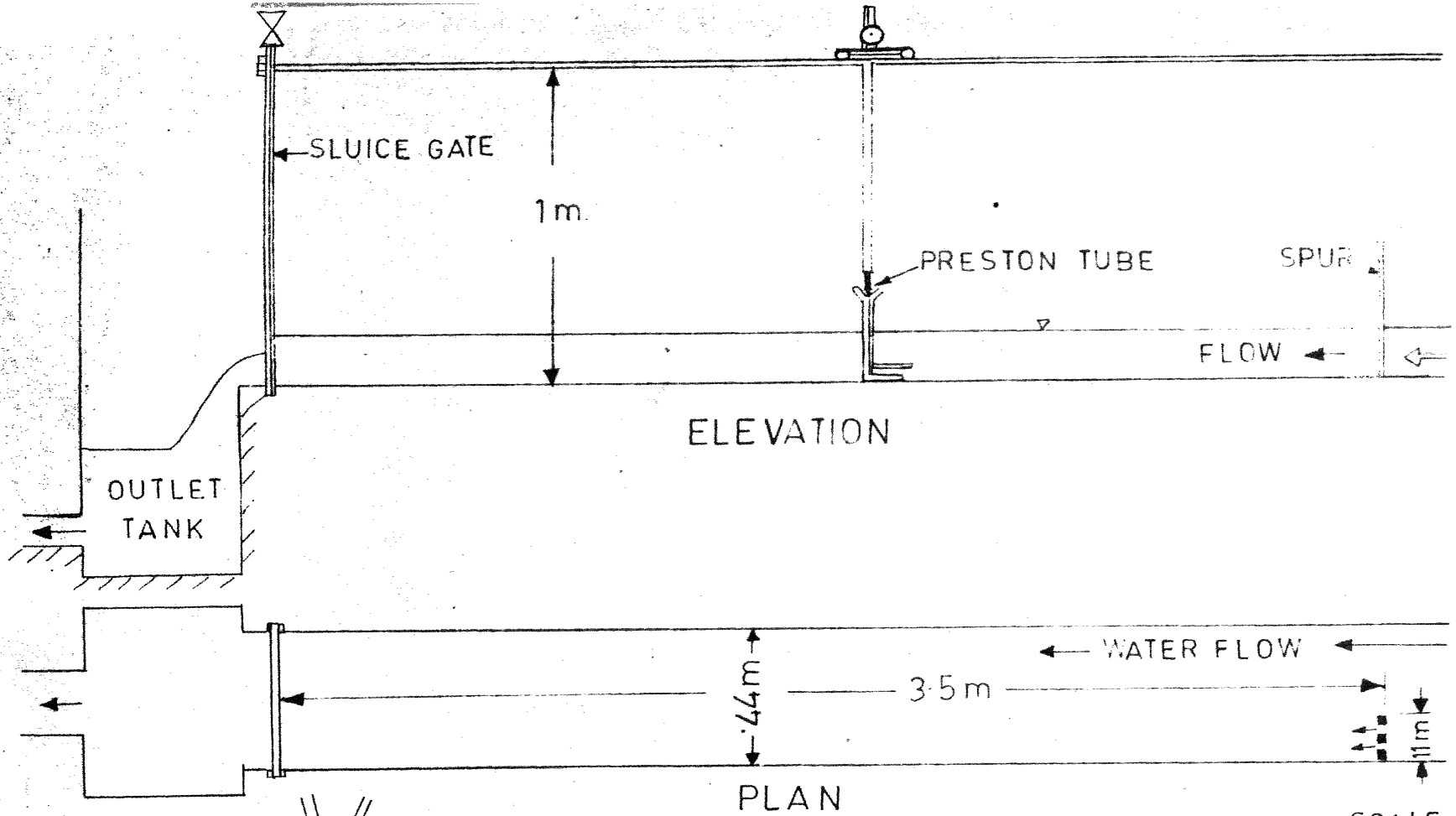

FIG.1. EXPERIMENTAL SET-UP

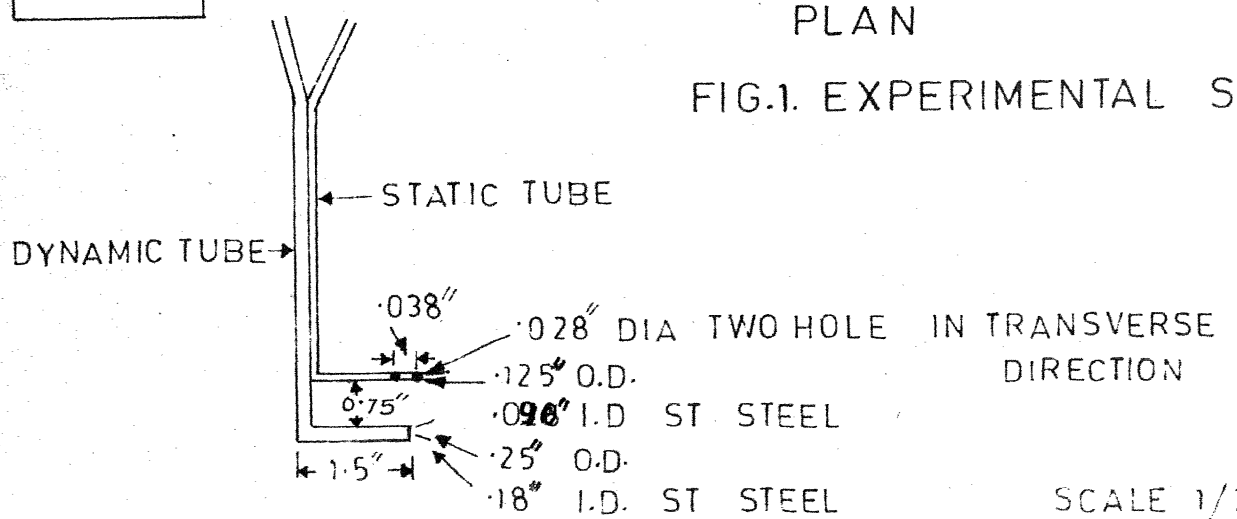

FIG·2. PRESTON TUBE

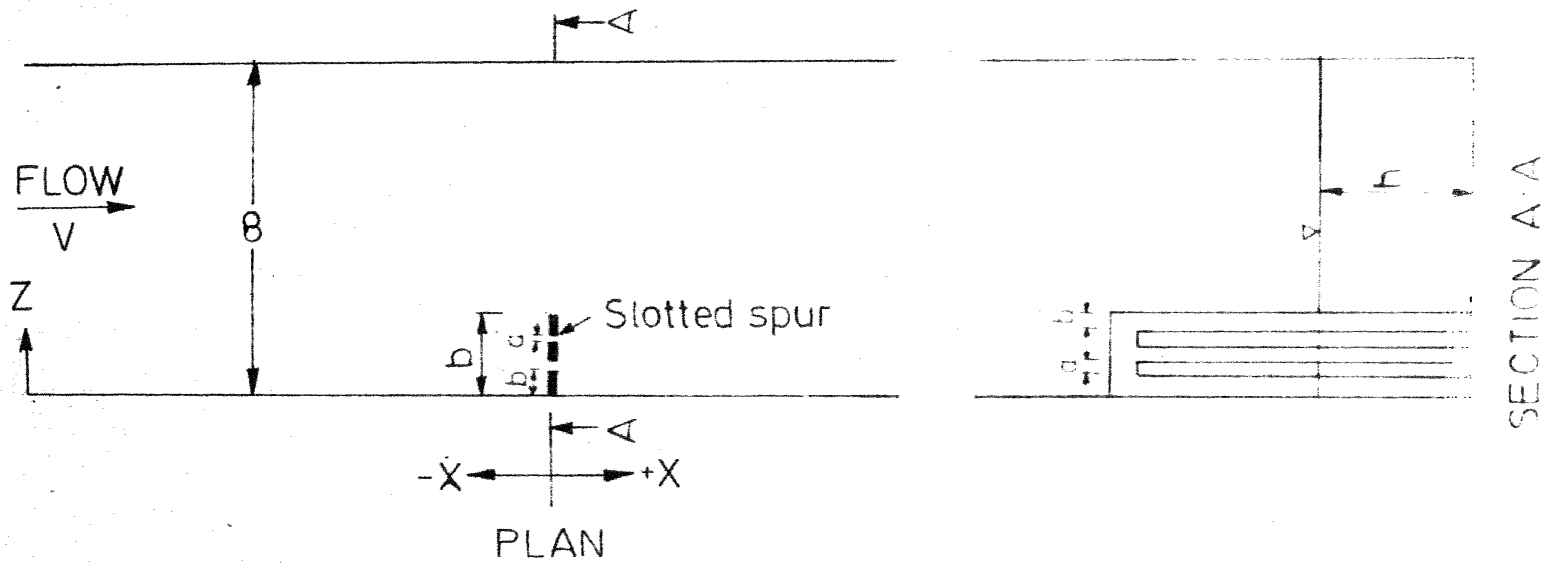

FIG.3 DEFINITION SKETCH

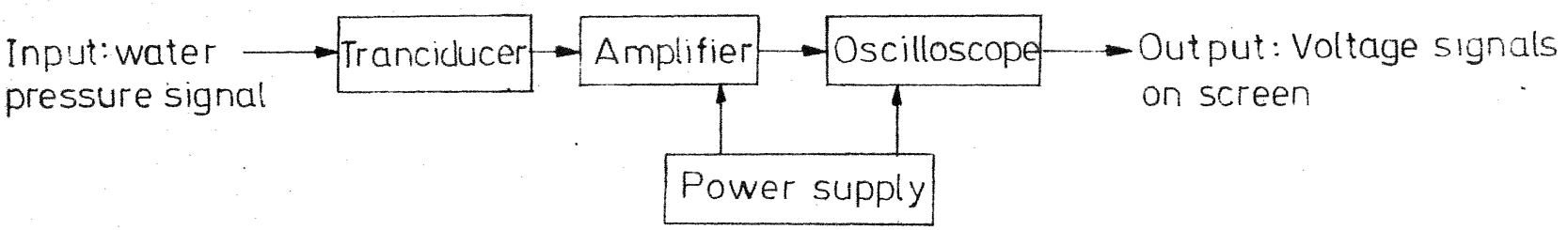

FIG. 4 OSCILLOSCOPE ASSEMBLY

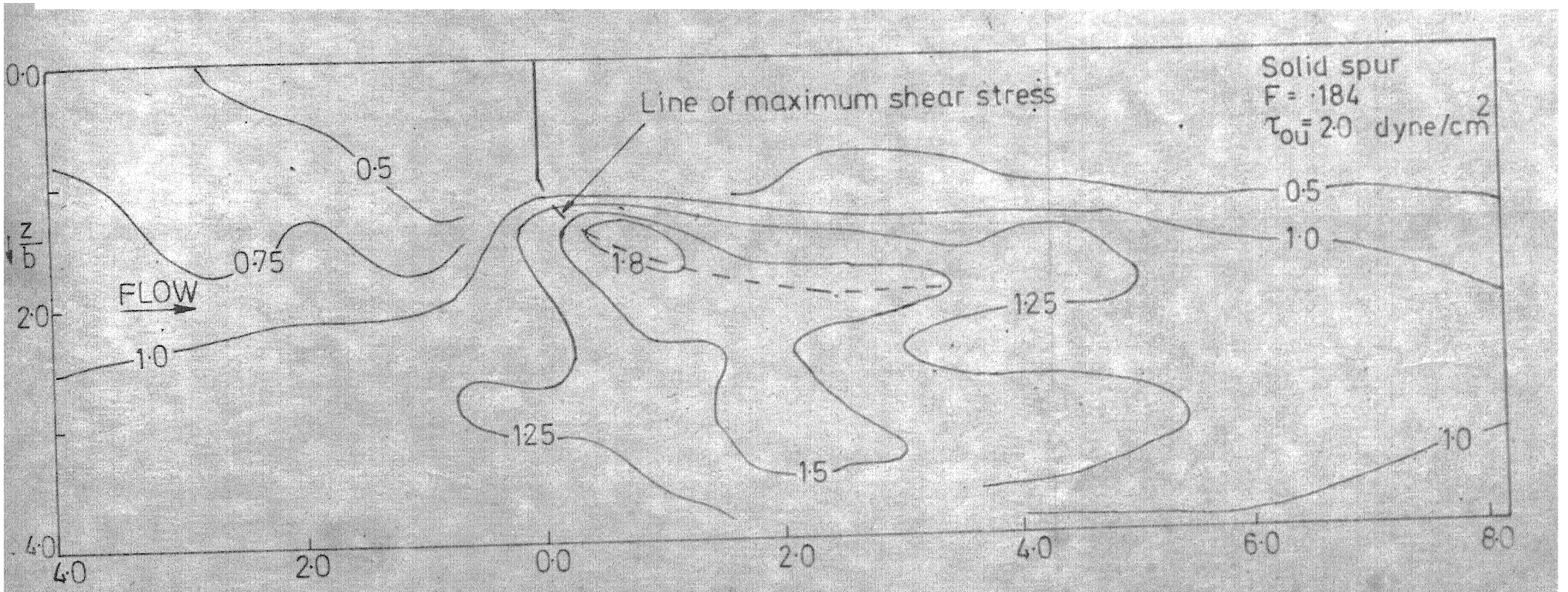

FIG. 5·1

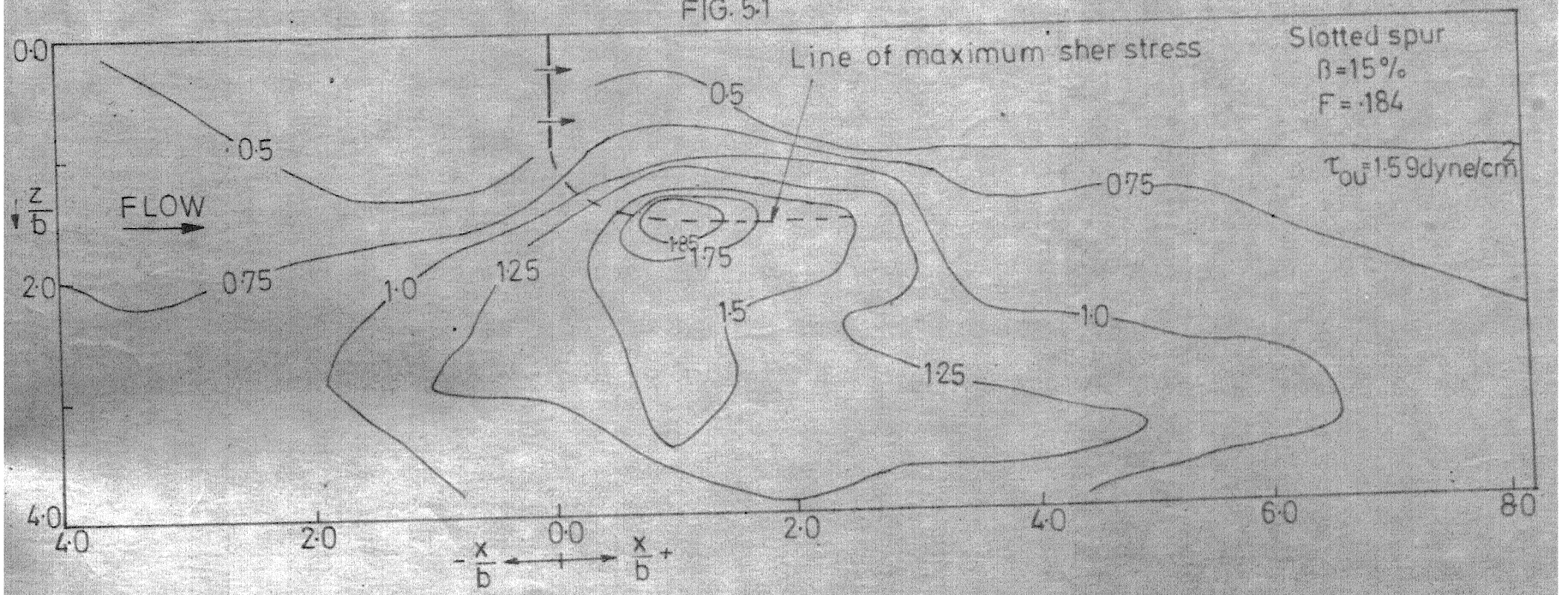

FIG.5·2 DISTRIBUTION OF BED SHEAR STRESS CONTOURS FOR F = ·184

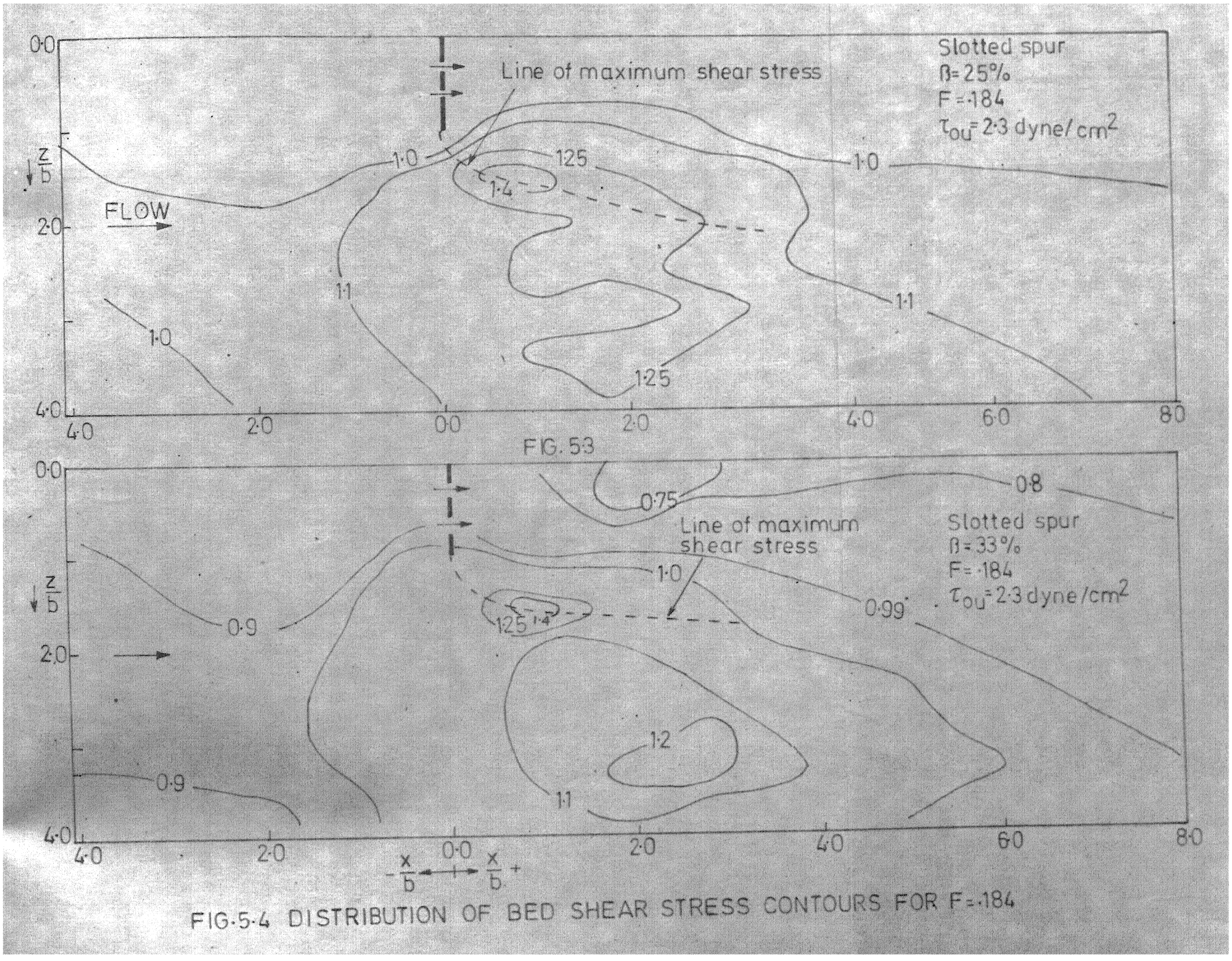

FIG. 5·3

FIG·5·4 DISTRIBUTION OF BED SHEAR STRESS CONTOURS FOR F = ·184

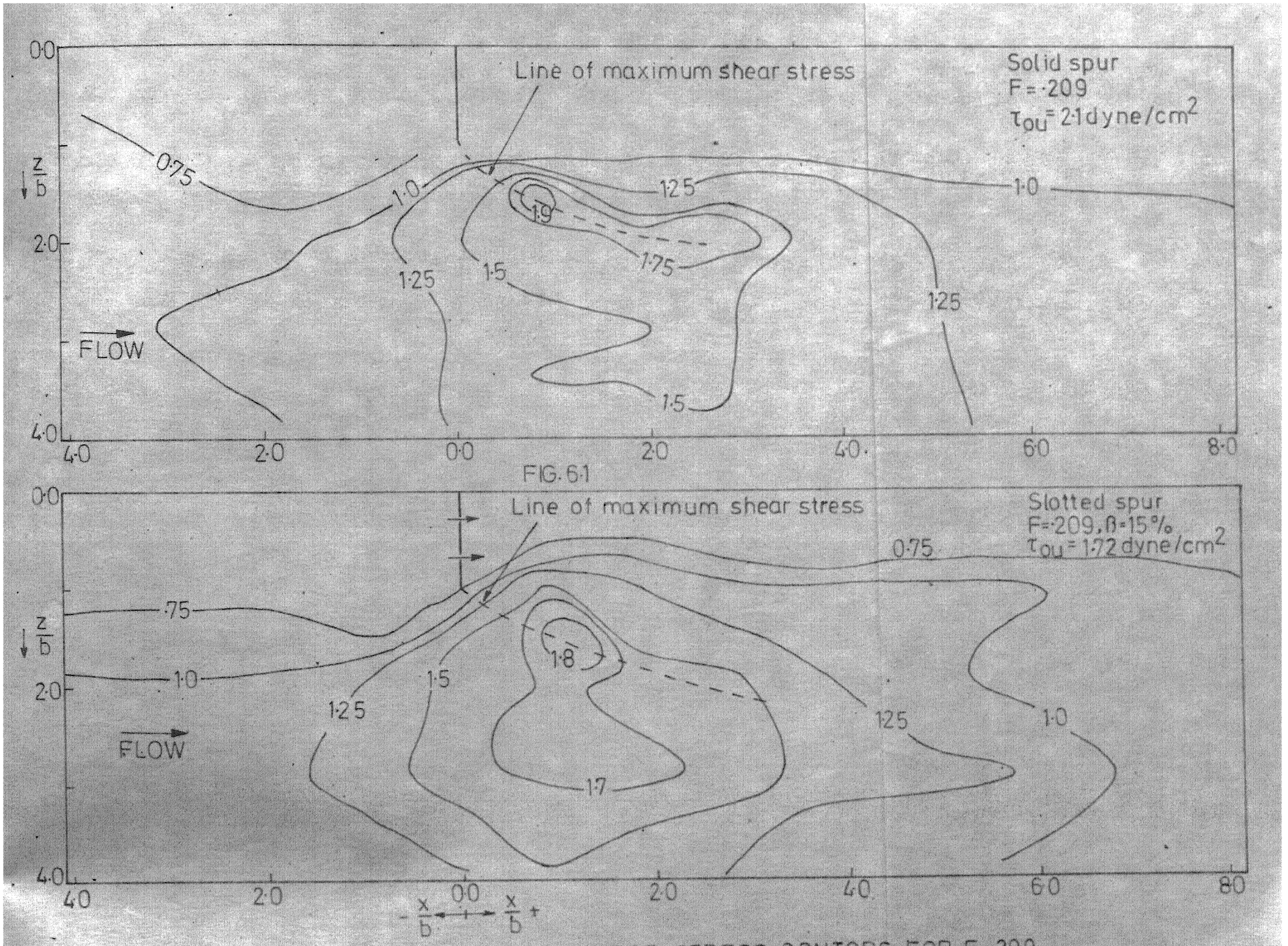

FIG. 6·1

FIG. 6·2 DISTRIBUTION OF BED SHEAR STRESS CONTORS FOR F=·209

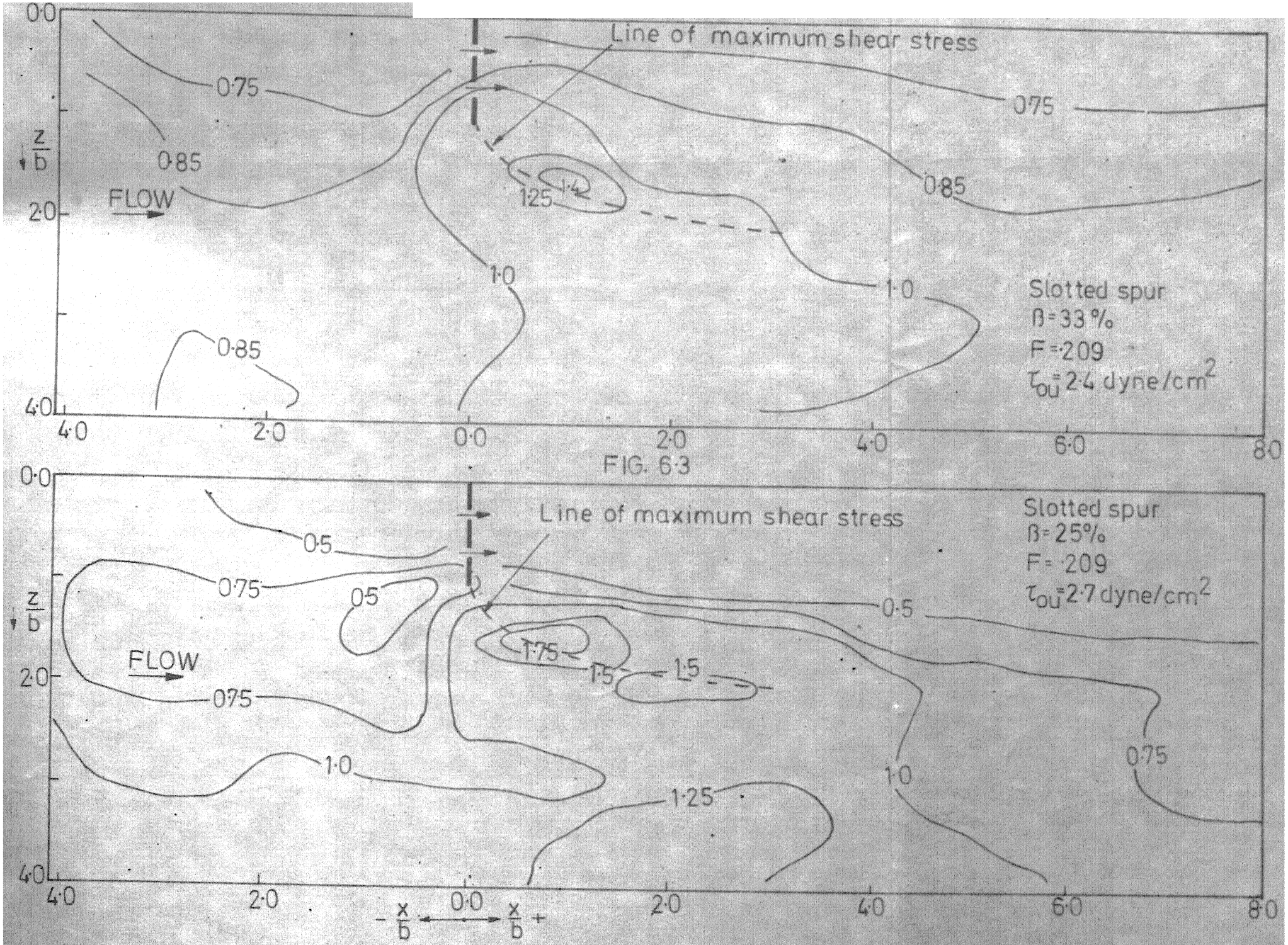

FIG. 6·3

FIG. 6·4 DISTRIBUTION OF BED SHEAR STRESS FOR F = ·209

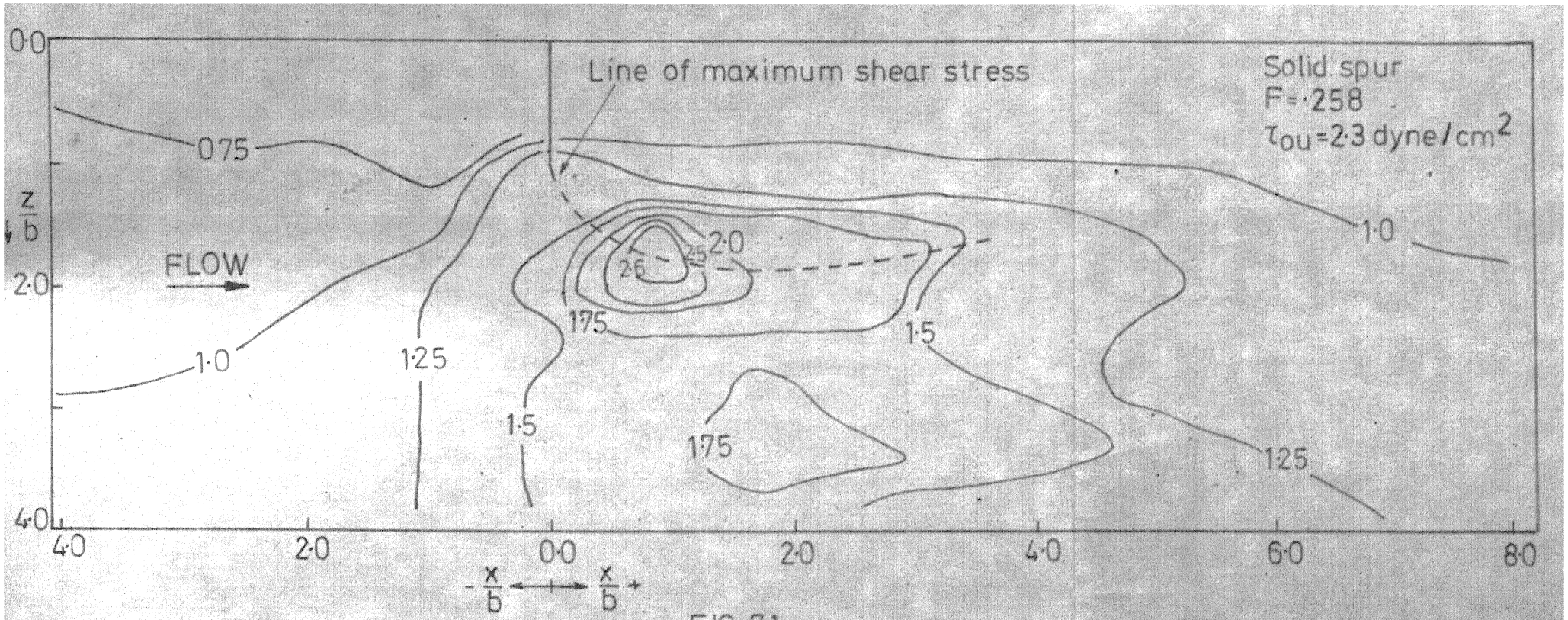

FIG. 7·1

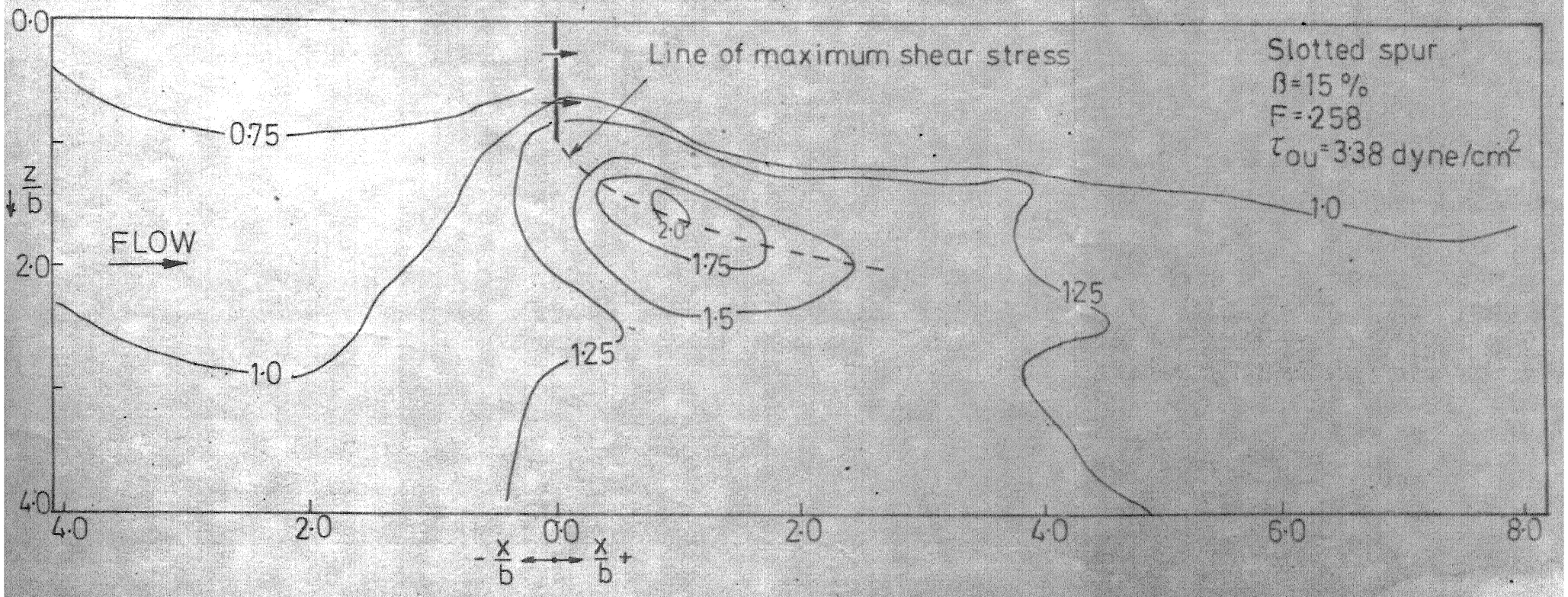

FIG·7·2 DISTRIBUTION OF BED SHEAR STRESS CONTOURS FOR F=·258

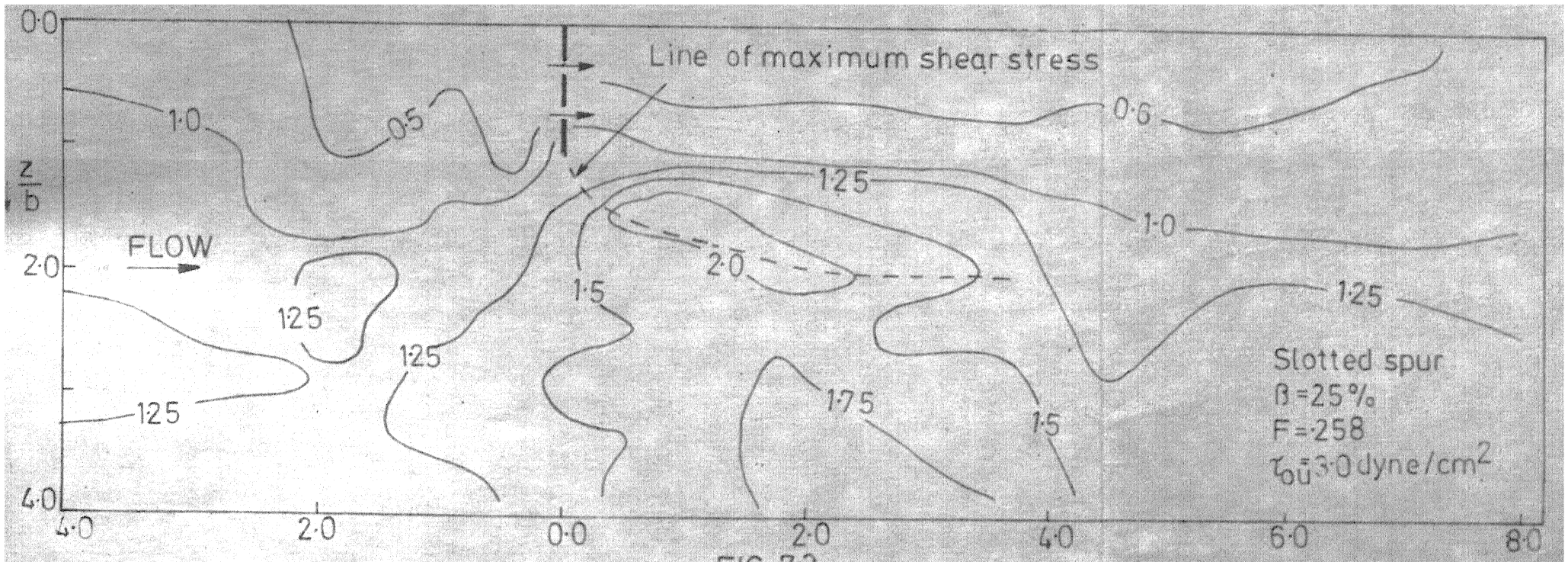

FIG. 7·3

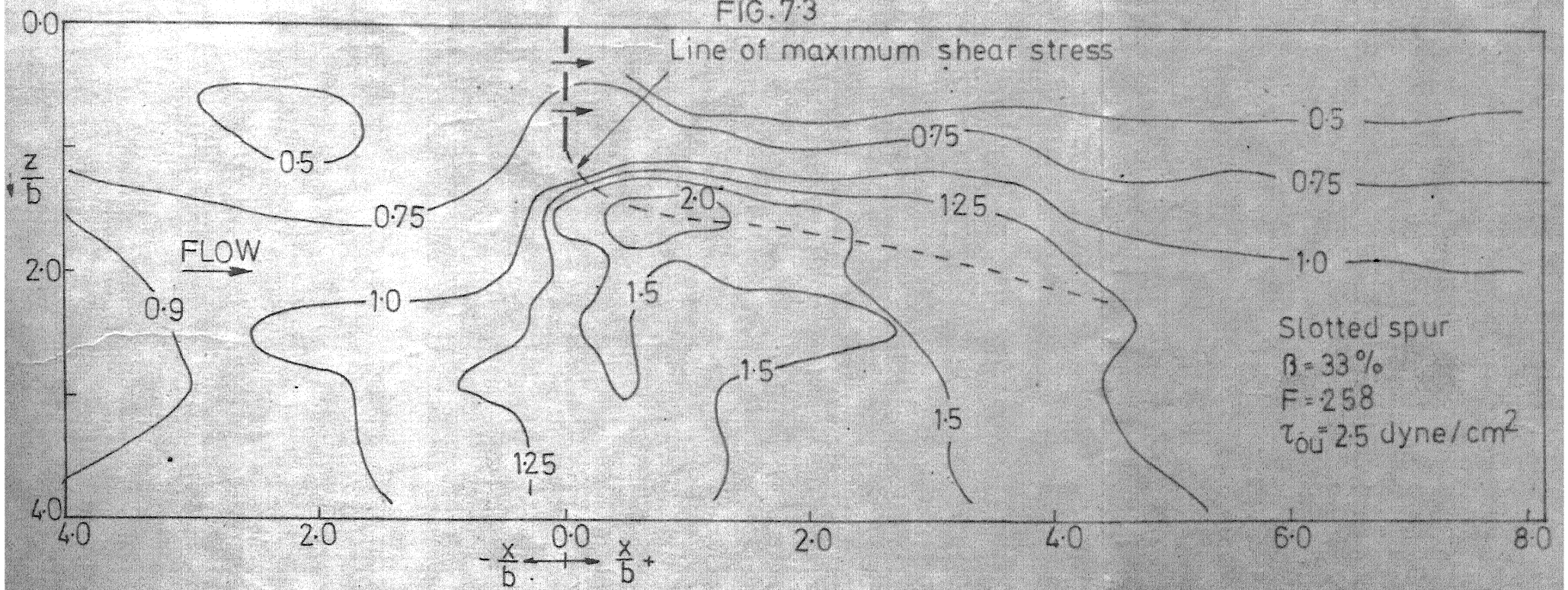

FIG·7·4 DISTRIBUTION OF BED SHEAR STRESS CONTOURS FOR F=·258

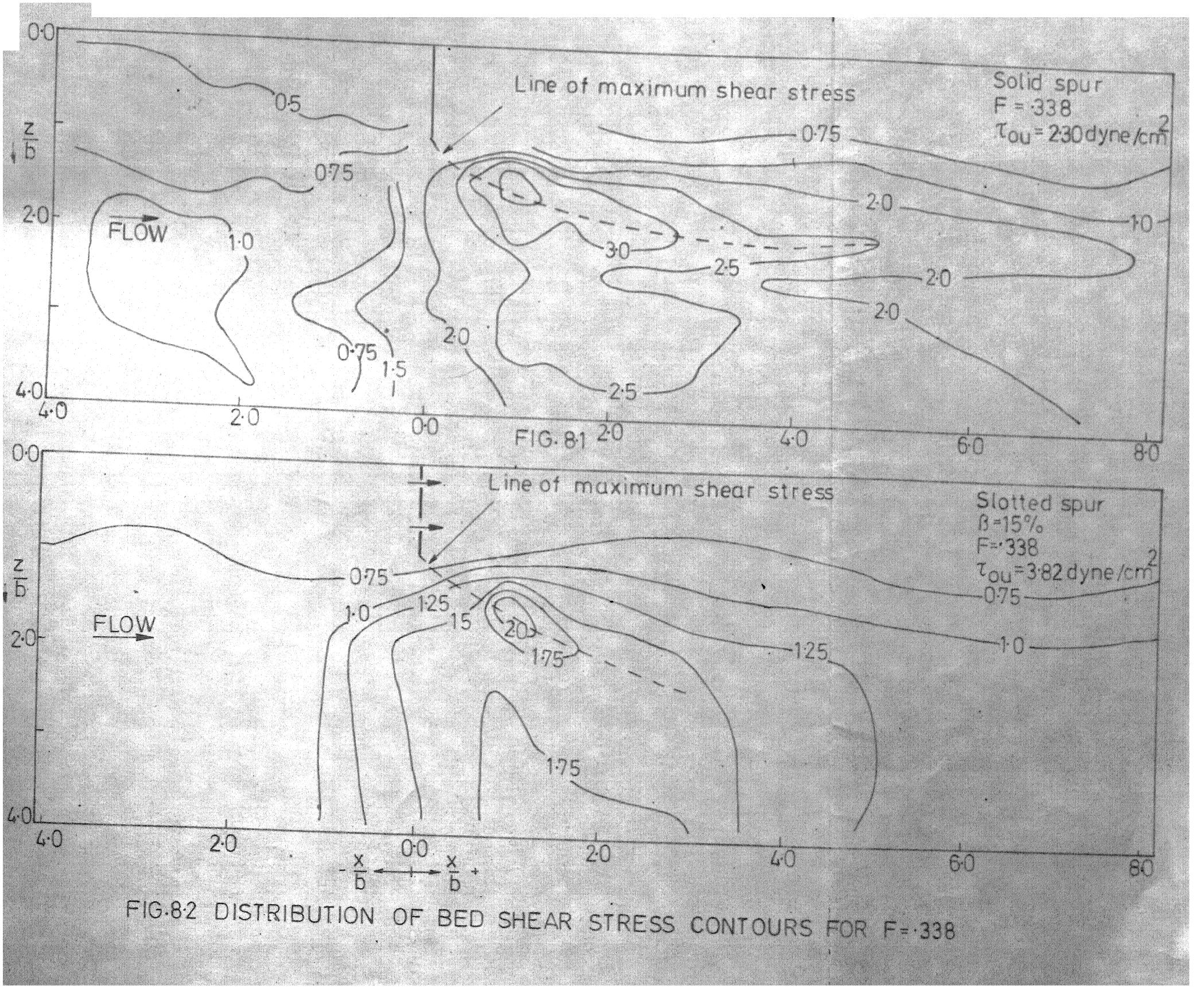

FIG. 8·1

FIG. 8·2 DISTRIBUTION OF BED SHEAR STRESS CONTOURS FOR F = ·338

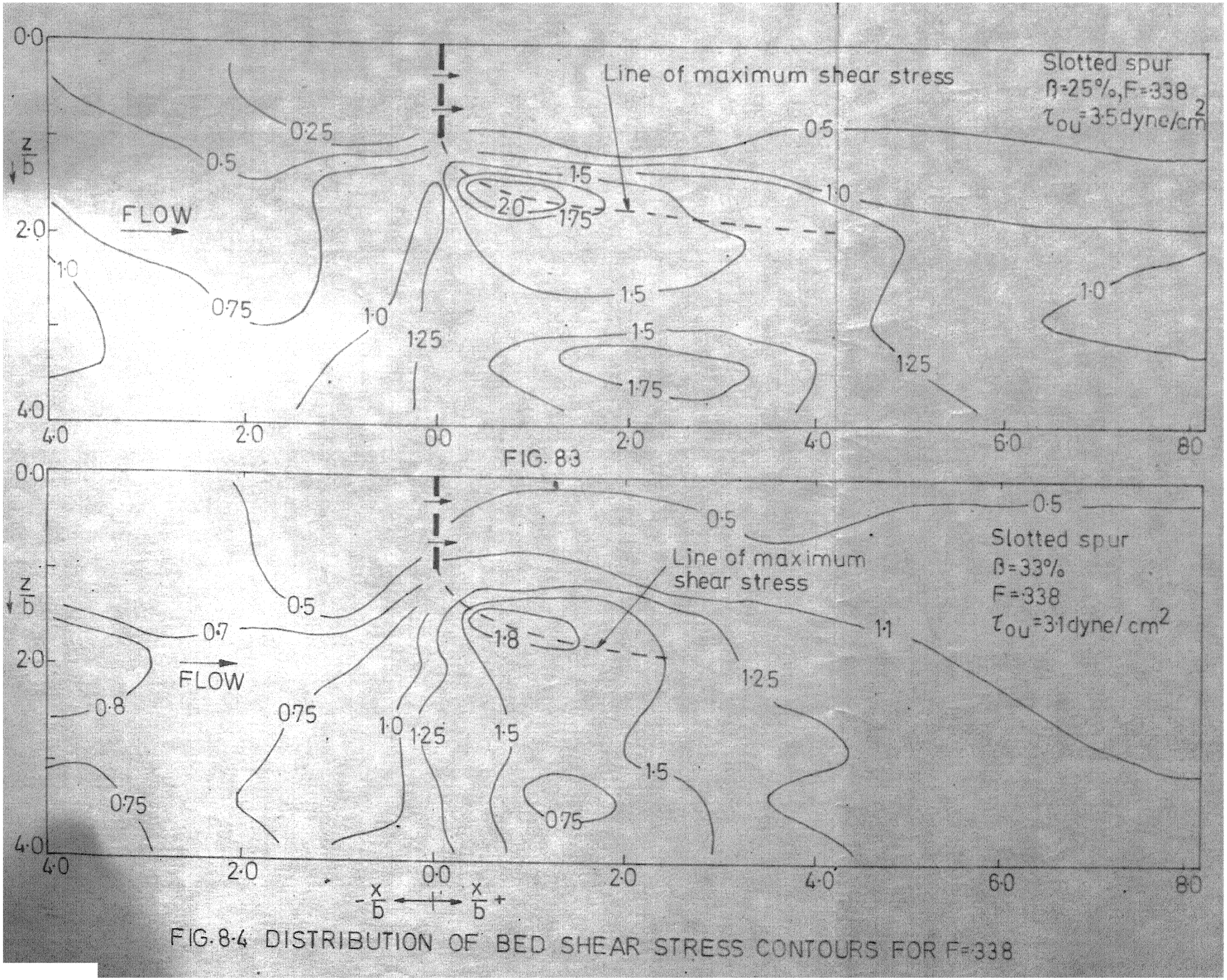

FIG. 8·3

FIG. 8·4 DISTRIBUTION OF BED SHEAR STRESS CONTOURS FOR F=·338

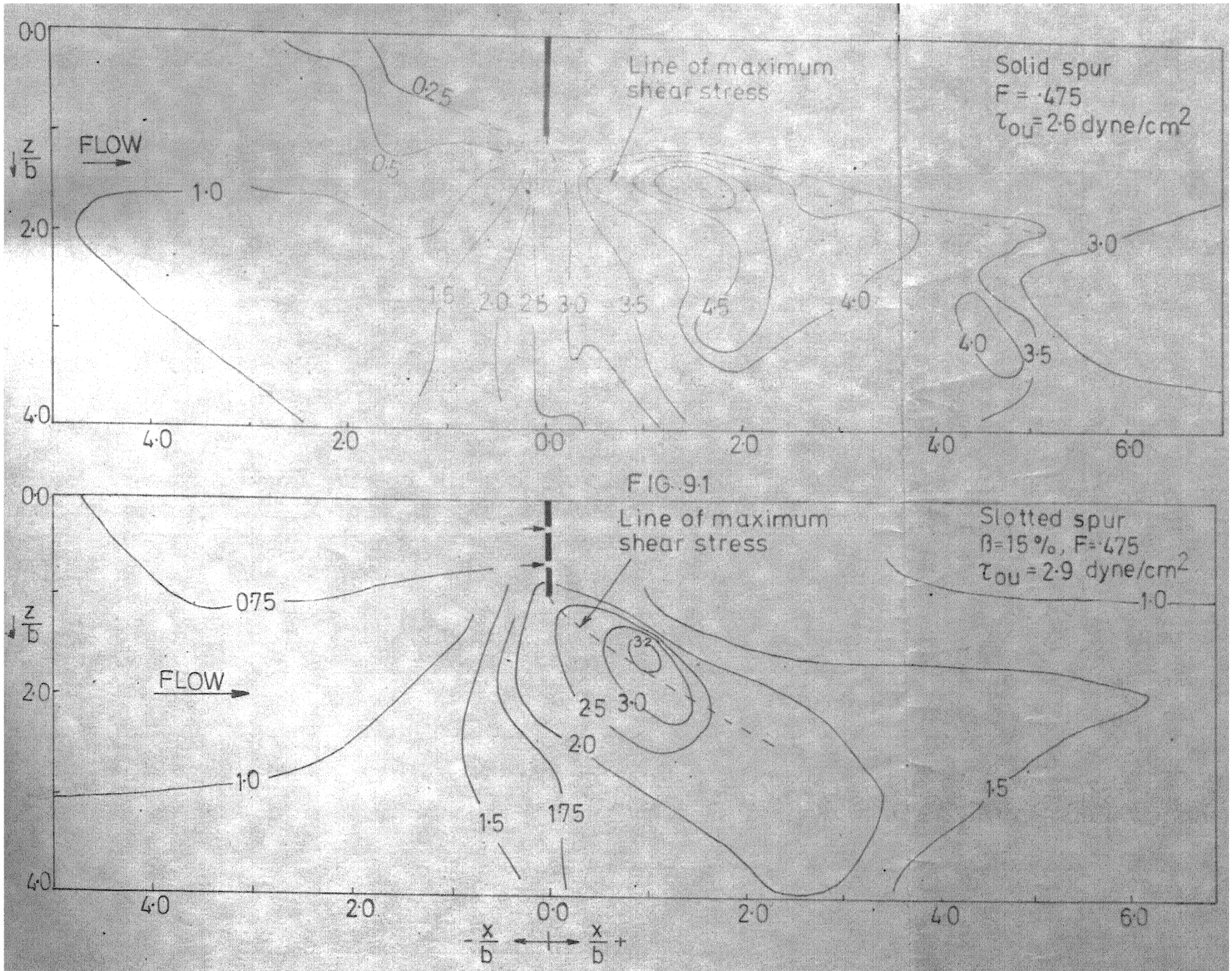

FIG·9·2 DISTRIBUTION OF BED SHEAR STRESS CONTOURS FOR DIFFERENT SPUR CONDITIONS
F = 0·475

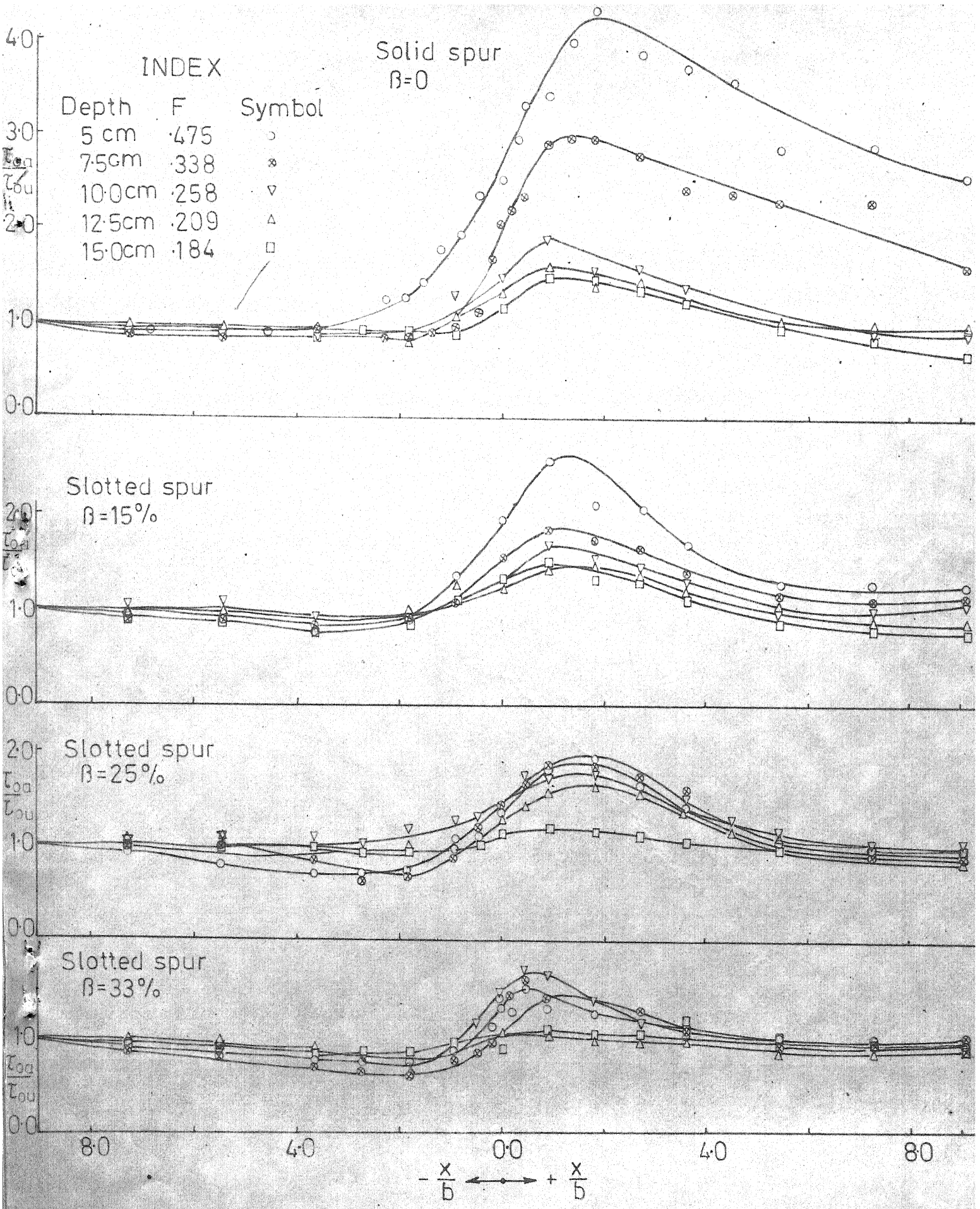

FIG·10 VARIATION OF AVERAGE SHEAR STRESS ALONG FLOW WITH DIFFERENT SPUR CONDITION

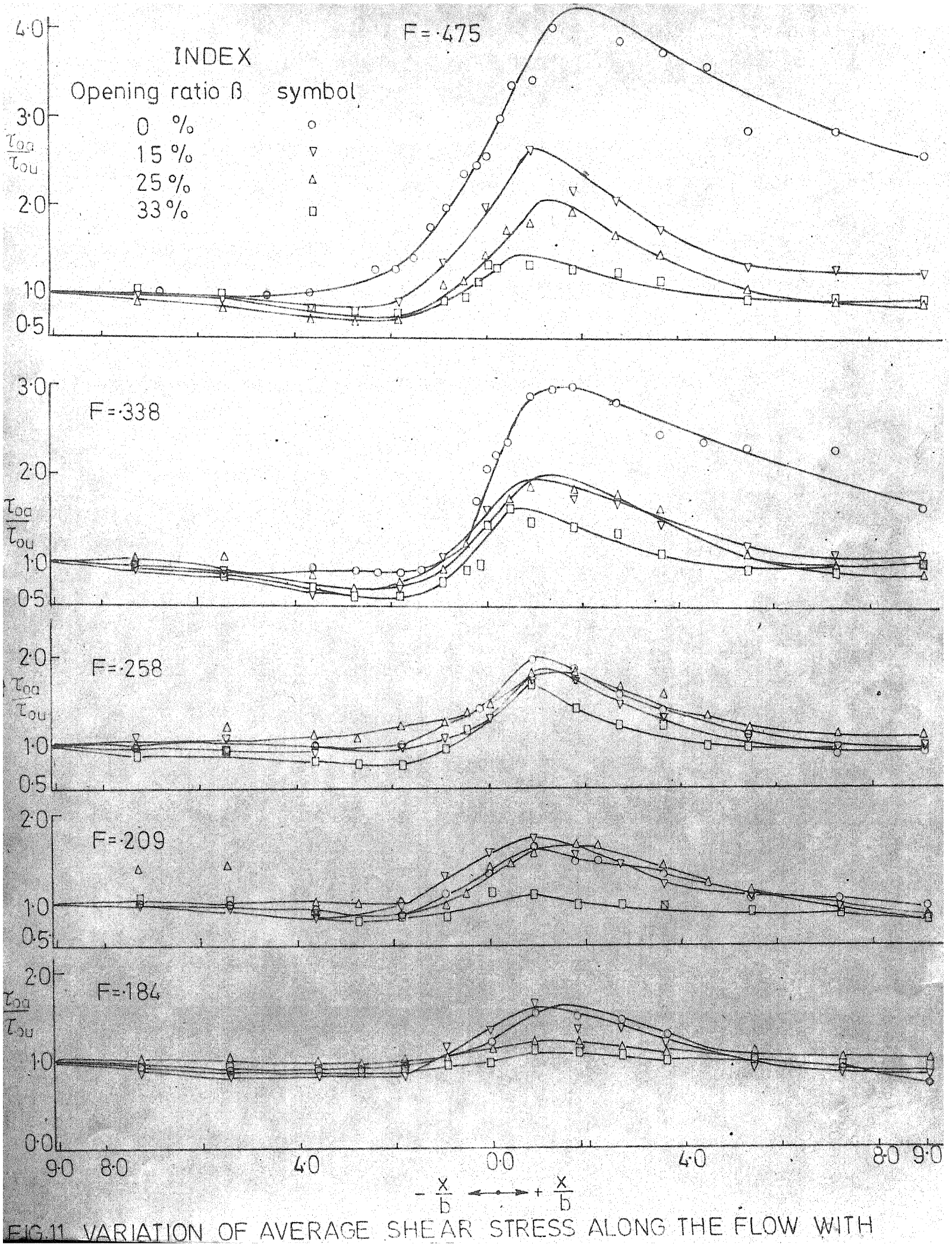

FIG.11 VARIATION OF AVERAGE SHEAR STRESS ALONG THE FLOW WITH

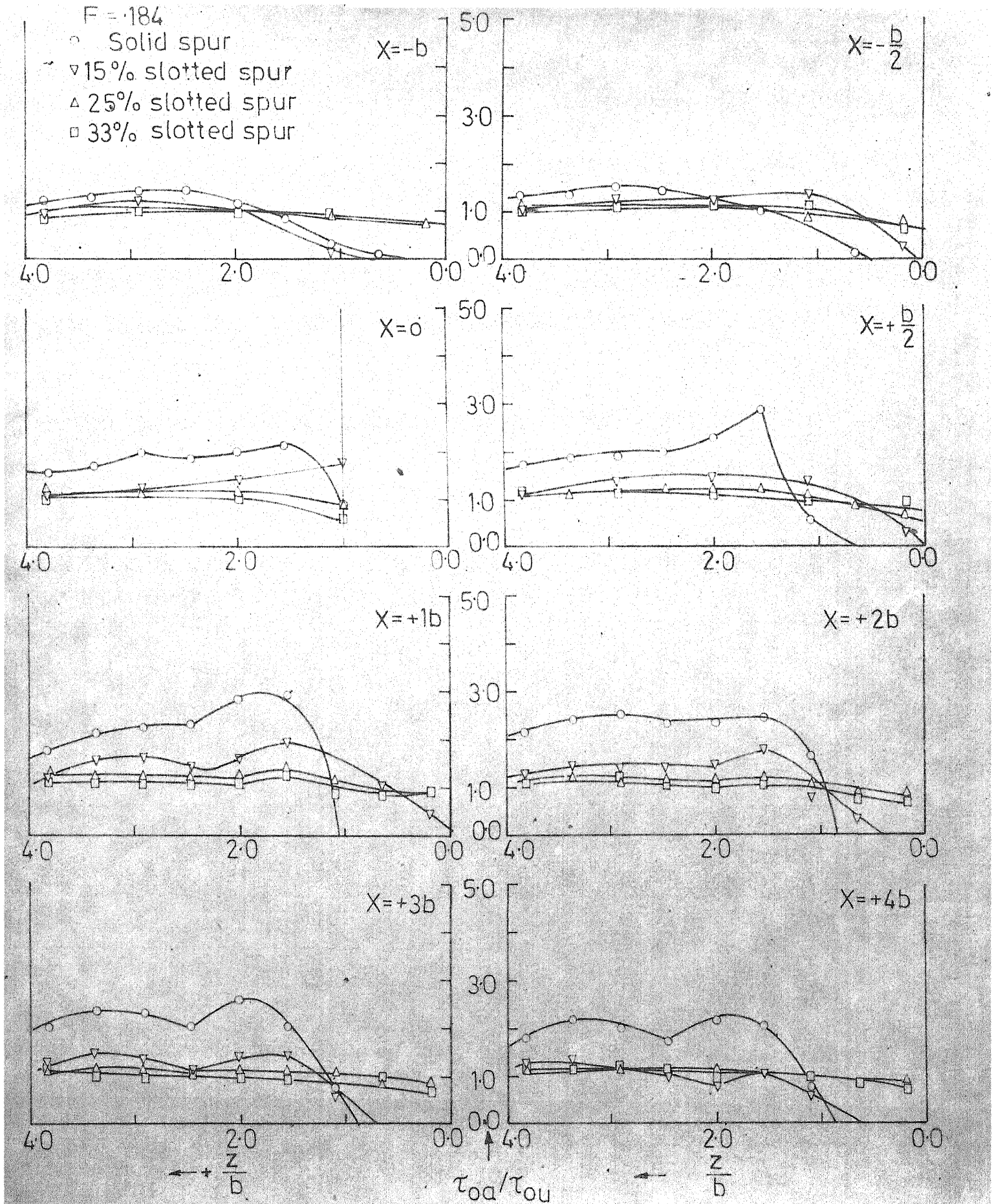

FIG·12 VARIATION OF BED SHEAR STRESS AT DIFFERENT FLOW CROSS SECTIONS

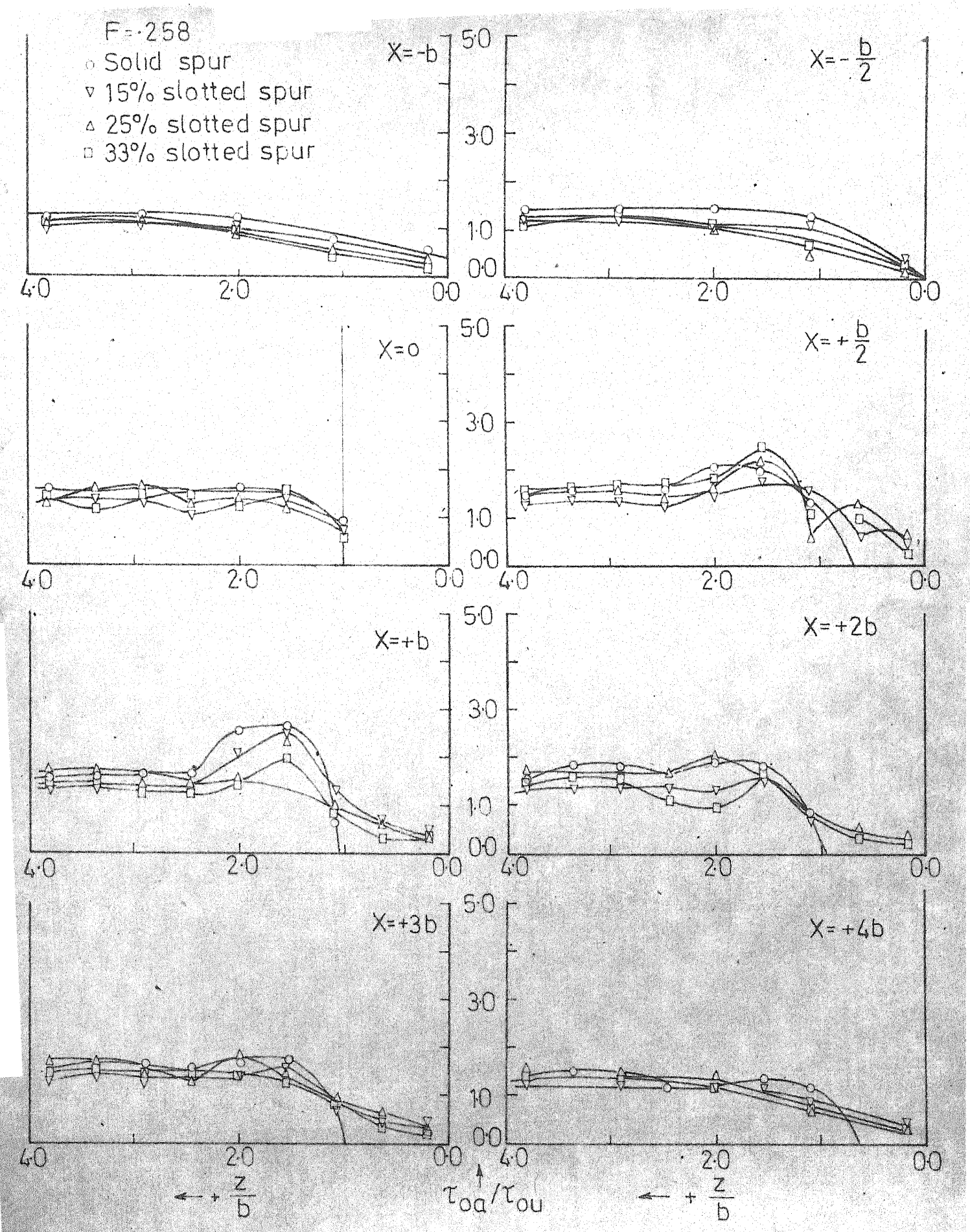

FIG·13 VARIATION OF BED SHEAR STRESS AT DIFFERENT FLOW CROSS SECTIONS

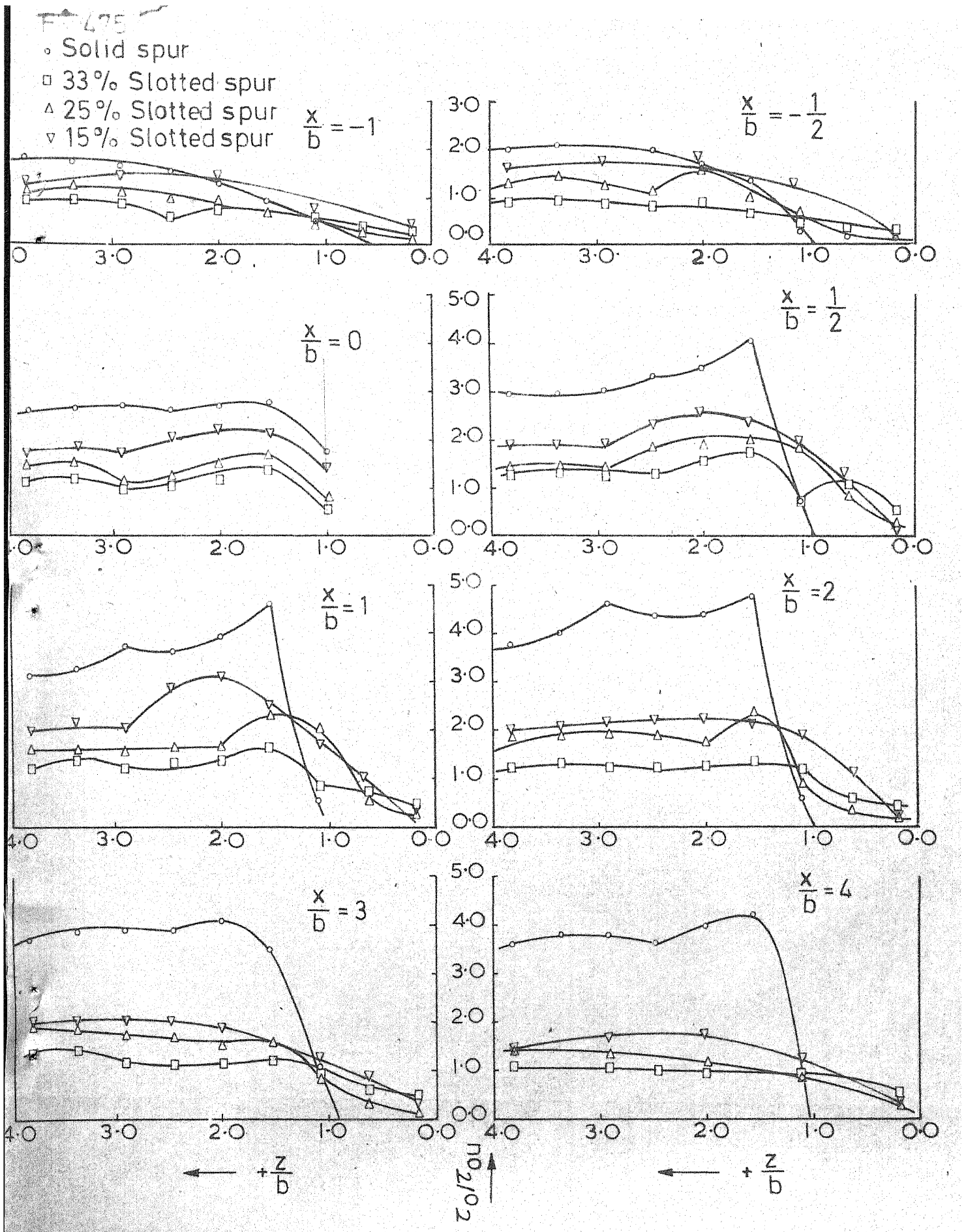

FIG.14 VARIATION OF BED SHEAR STRESS AT DIFFERENT FLOW CROSS SECTIONS

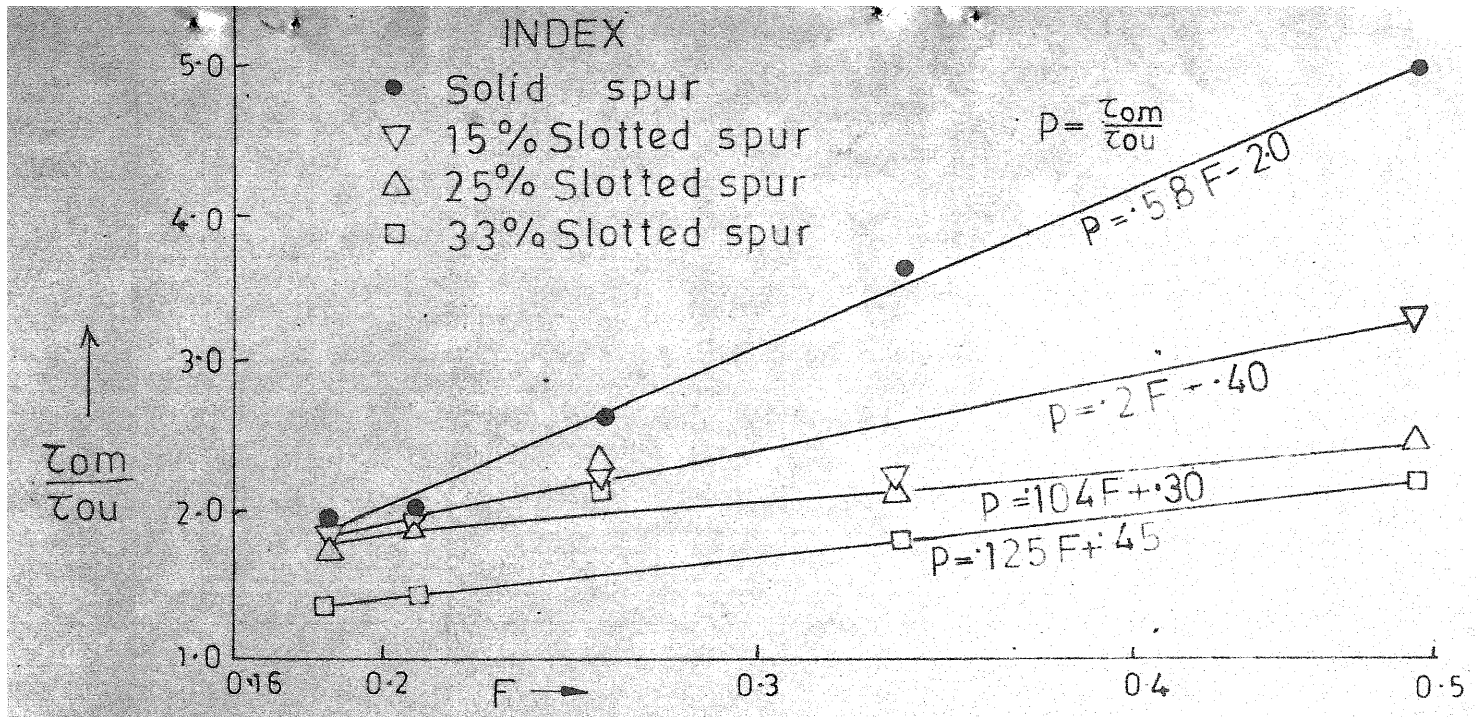

FIG.15 VARIATION OF MAXIMUM SHEAR STRESS WITH FROUDE NUMBER

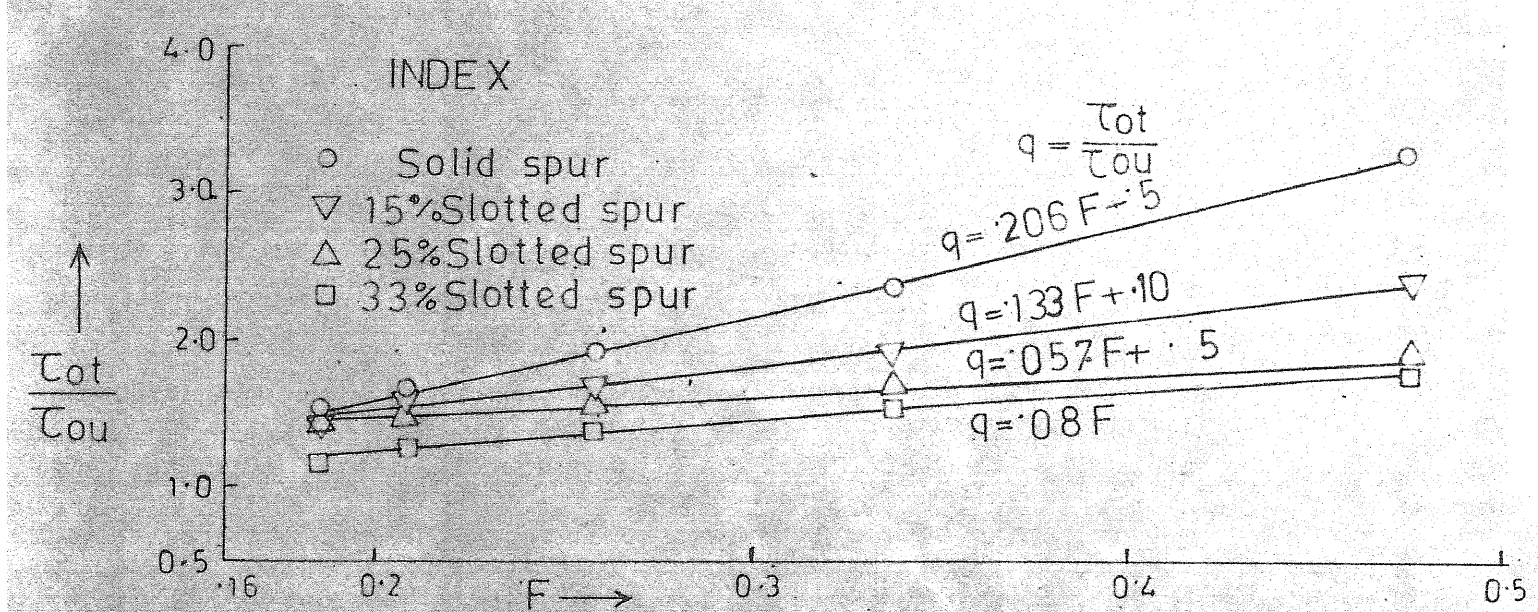

FIG.16 VARIATION OF SHEAR STRESS AT TIP WITH FROUDE NUMBER

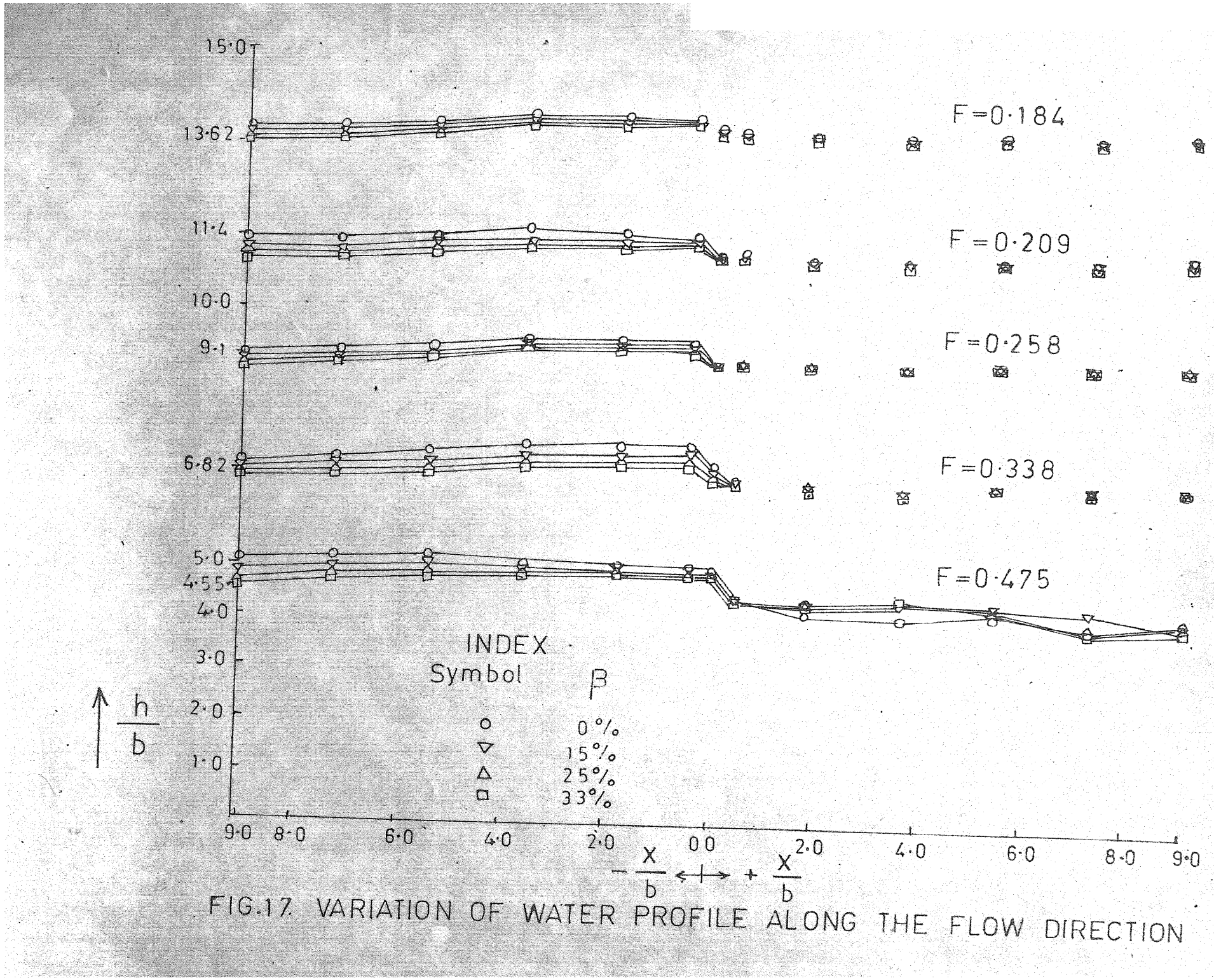

FIG.17. VARIATION OF WATER PROFILE ALONG THE FLOW DIRECTION

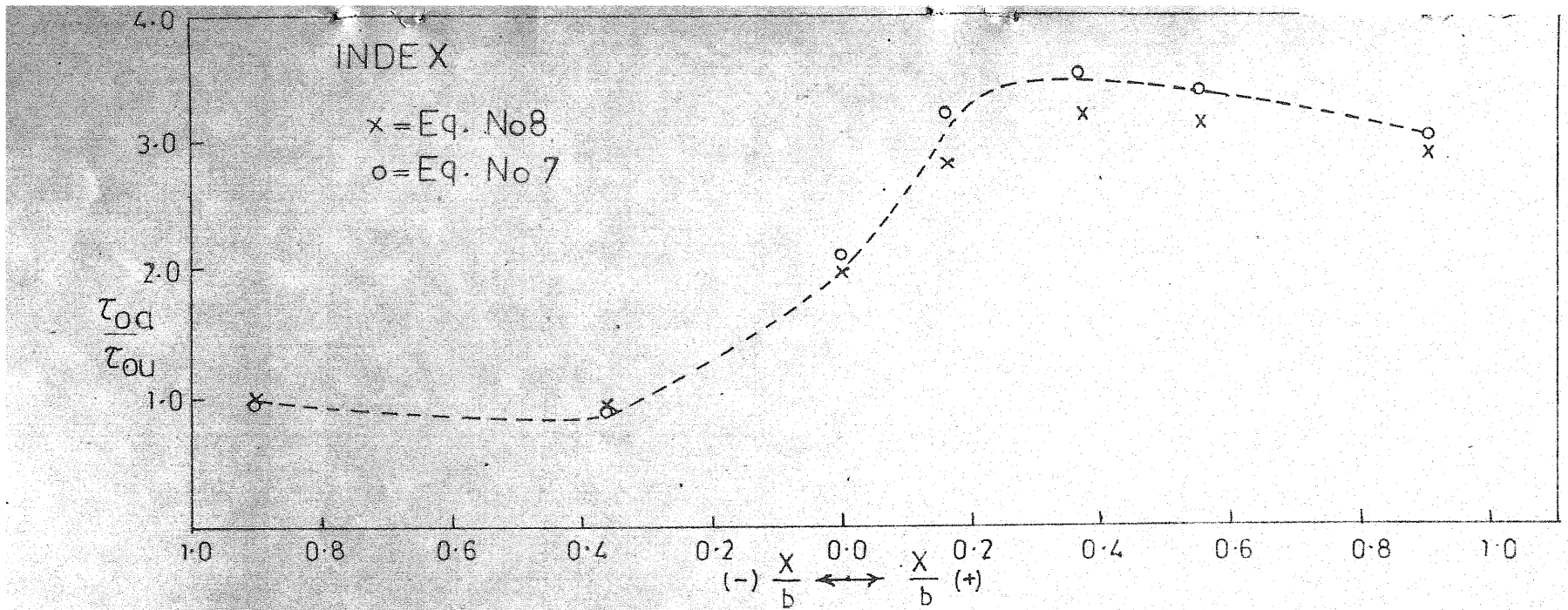

FIG.18. COMPARISION OF EQUATIONS NO. 7 AND 8

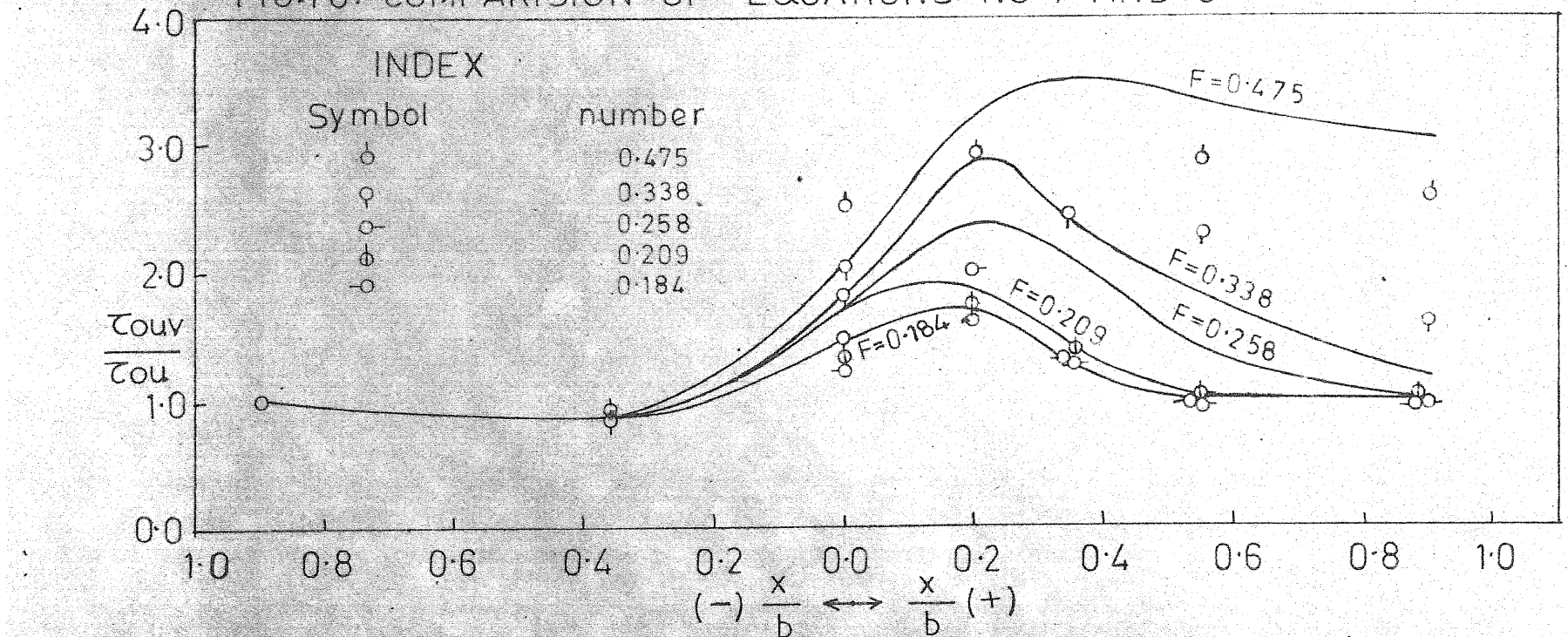

FIG.19. COMPARISION OF EQUATION 8 WITH EXPERIMENTAL OBSERVATION

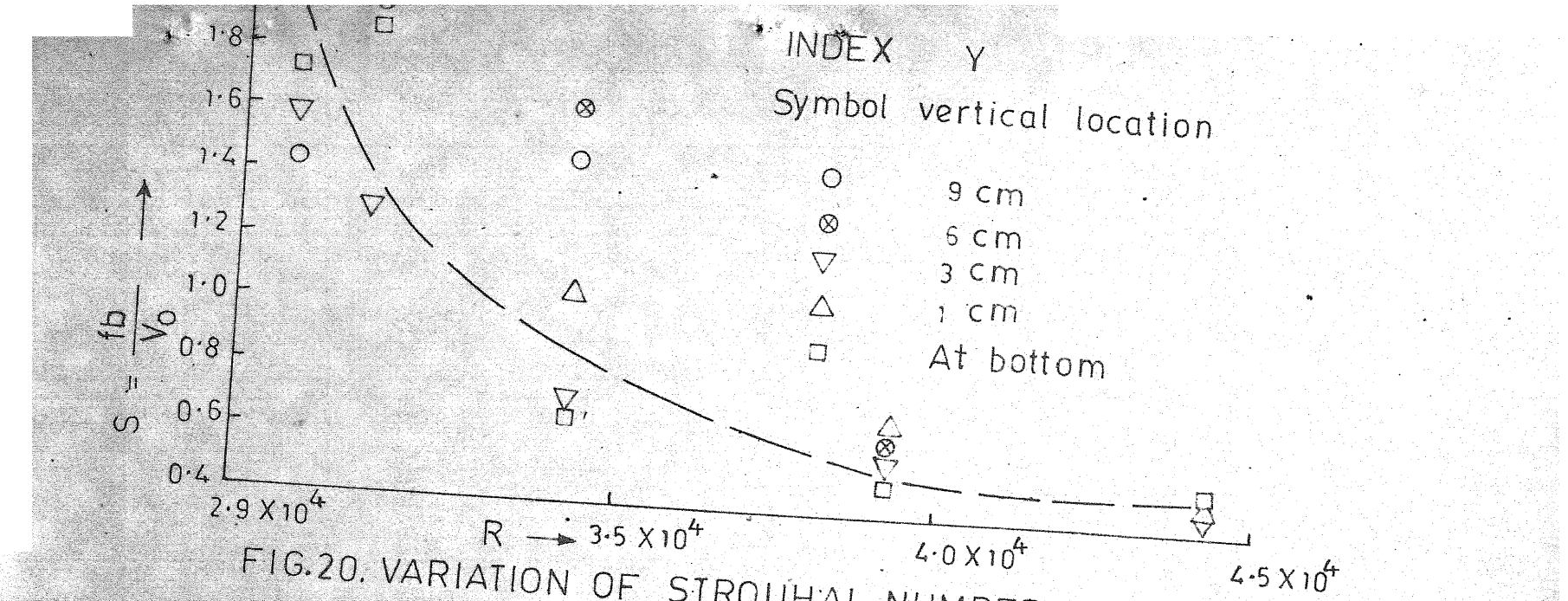

FIG.20. VARIATION OF STROUHAL NUMBER WITH REYNOD NUMBER

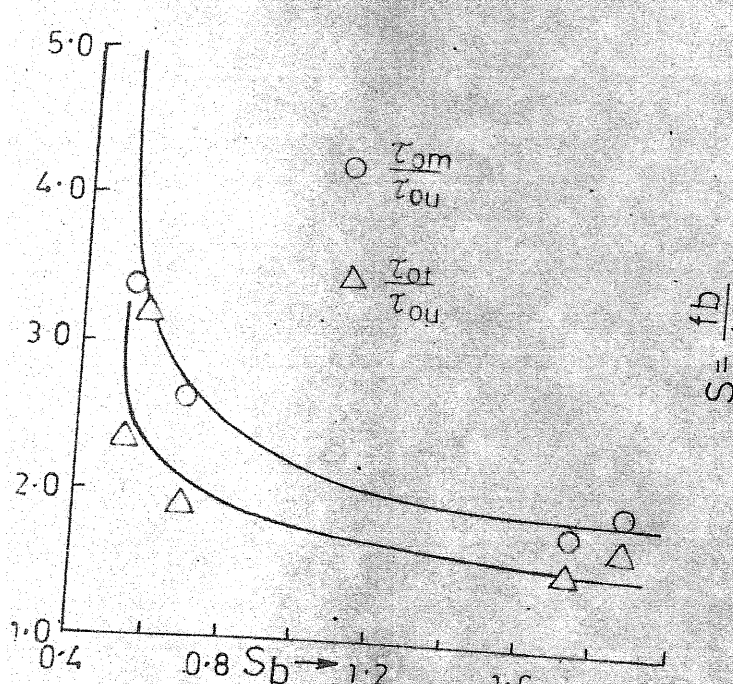

FIG.22. VARIATION OF BOTTOM STROUHAL NUMBER WITH SHEAR STRESS

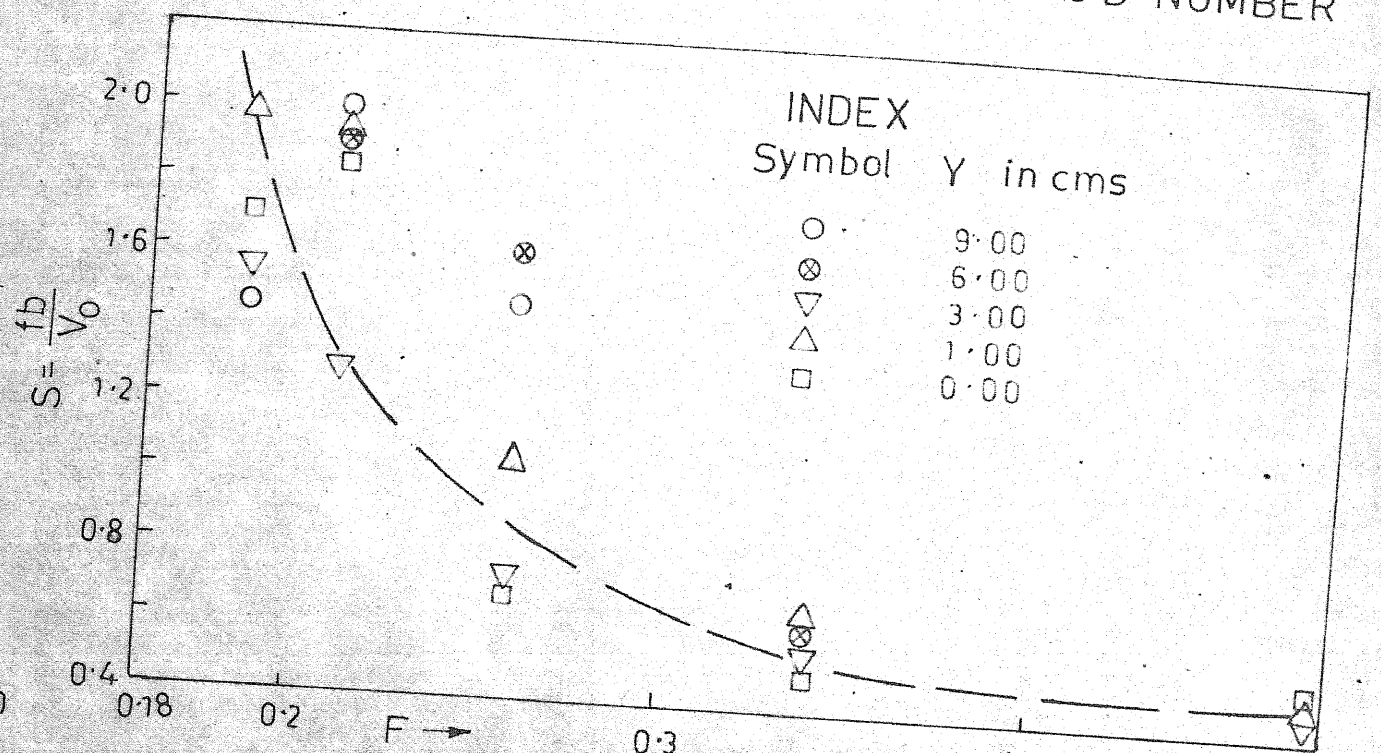

FIG.21. VARIATION OF FROUDE NUMBER WITH STROUHAL NUMBER

F = ·475
V. POSITION : BOTTOM
H. SCALE : .2 sec/cm
V. SCALE : .5 volt/cm

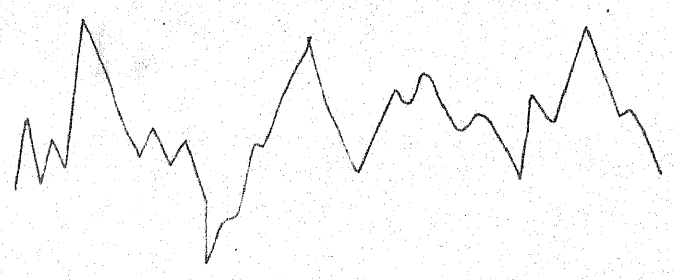

F = ·338
V. POSITION: BOTTOM
H. SCALE : .2sec/cm
V. SCALE: .5 volt/cm

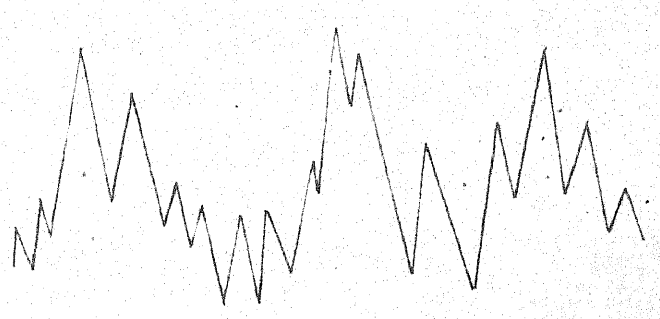

F = ·258
V. POSITION: 3cm from bottom
H. SCALE : .2sec/cm
V. SCALE : ·5volt/cm

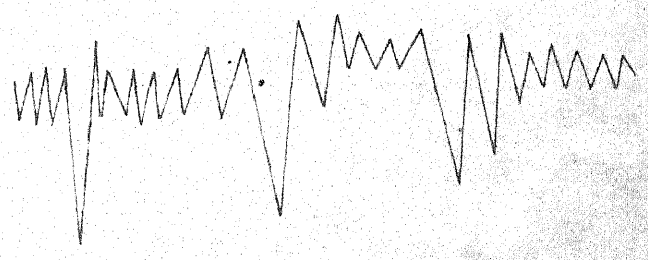

F = ·258
V. POSITION: 9cm from bottom
H. SCALE : .1sec/cm
V. SCALE : .1volt/cm

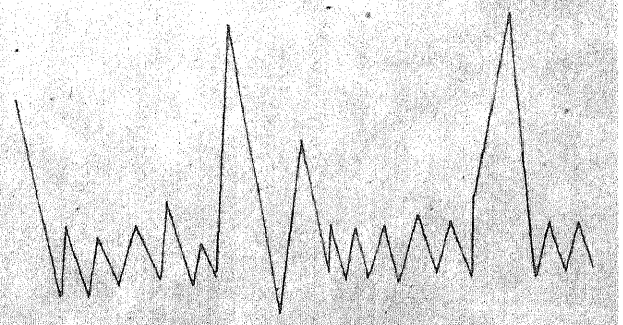

F = ·184
V. POSITION : 1cm from bottom
H. SCALE : .1sec/cm
V. SCALE : .5volt/cm

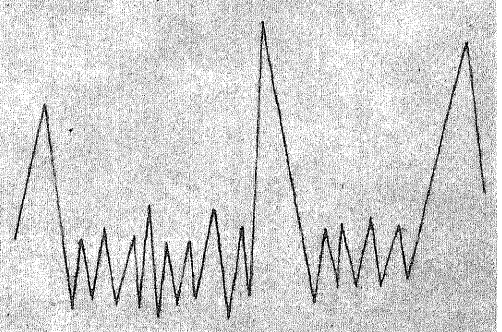

FIG·23 SCREEN DISPLAY OF VORTICES MEASUREMENTS FOR SOLID SPUR

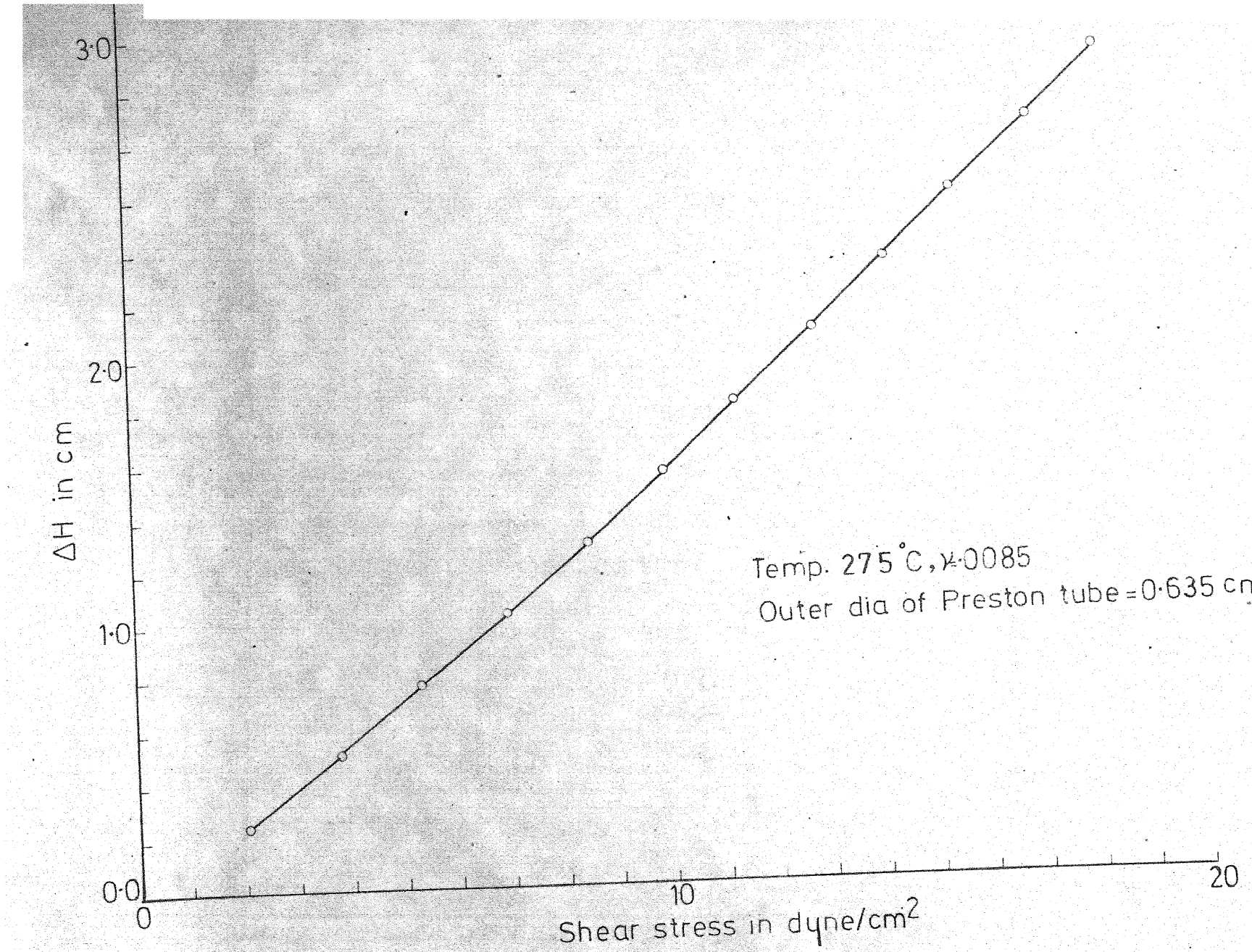

FIG. 24 CALIBRATION CURVE FOR PRESTON TUBE

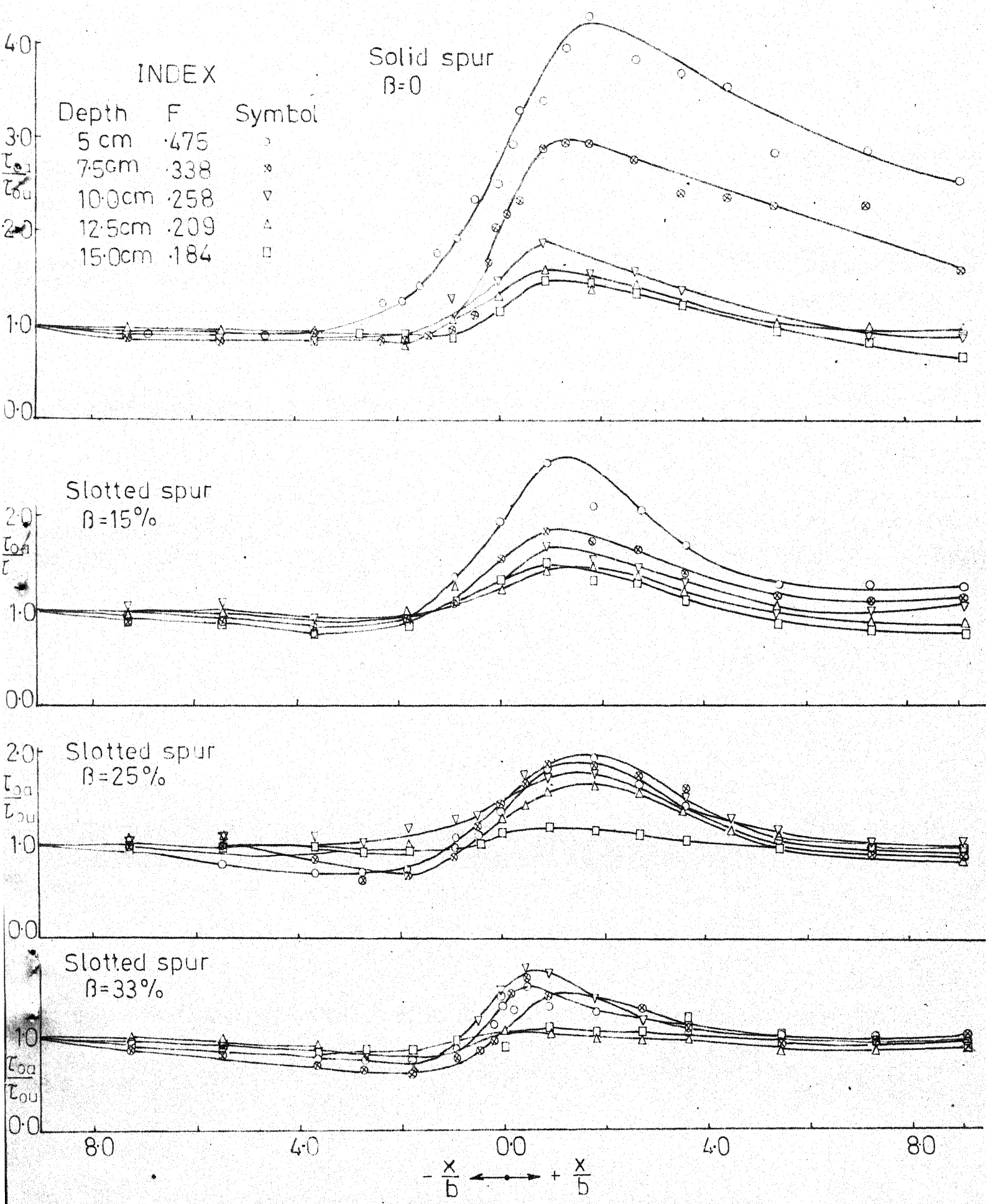

FIG·10 VARIATION OF AVERAGE SHEAR STRESS ALONG FLOW WITH DIFFERENT SPUR CONDITION

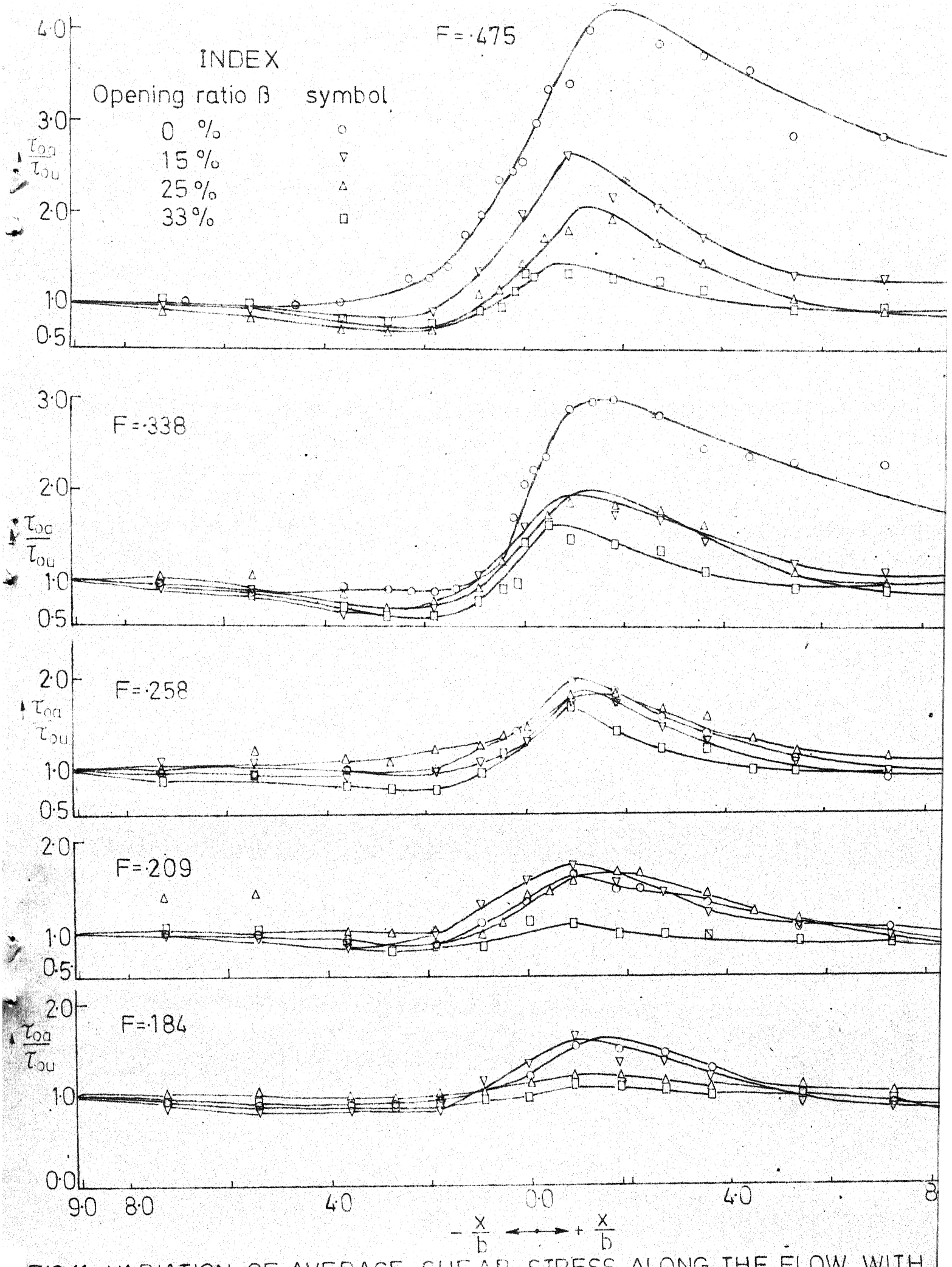

FIG.11 VARIATION OF AVERAGE SHEAR STRESS ALONG THE FLOW WITH

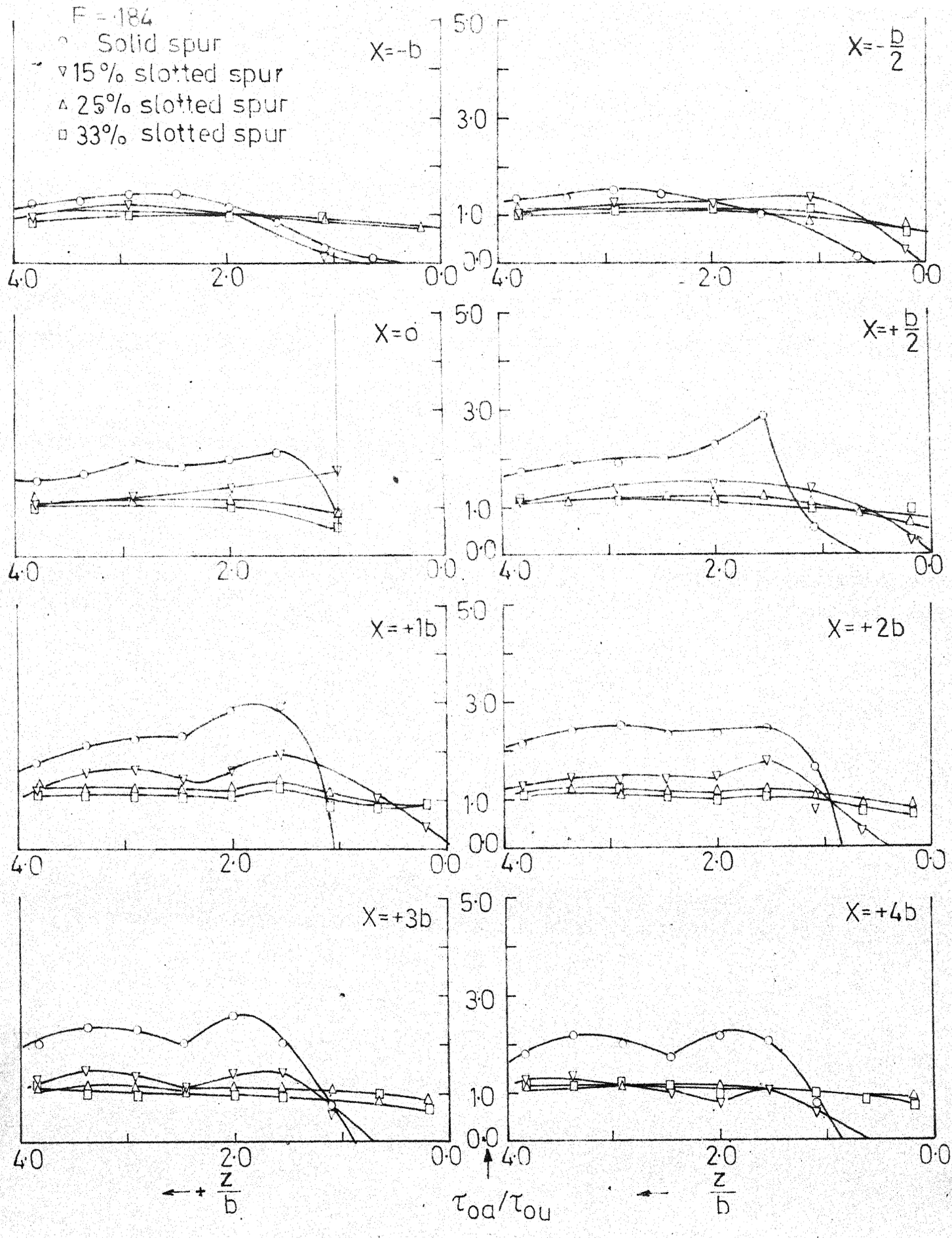

FIG·12 VARIATION OF BED SHEAR STRESS AT DIFFERENT FLOW CROSS SECTIONS

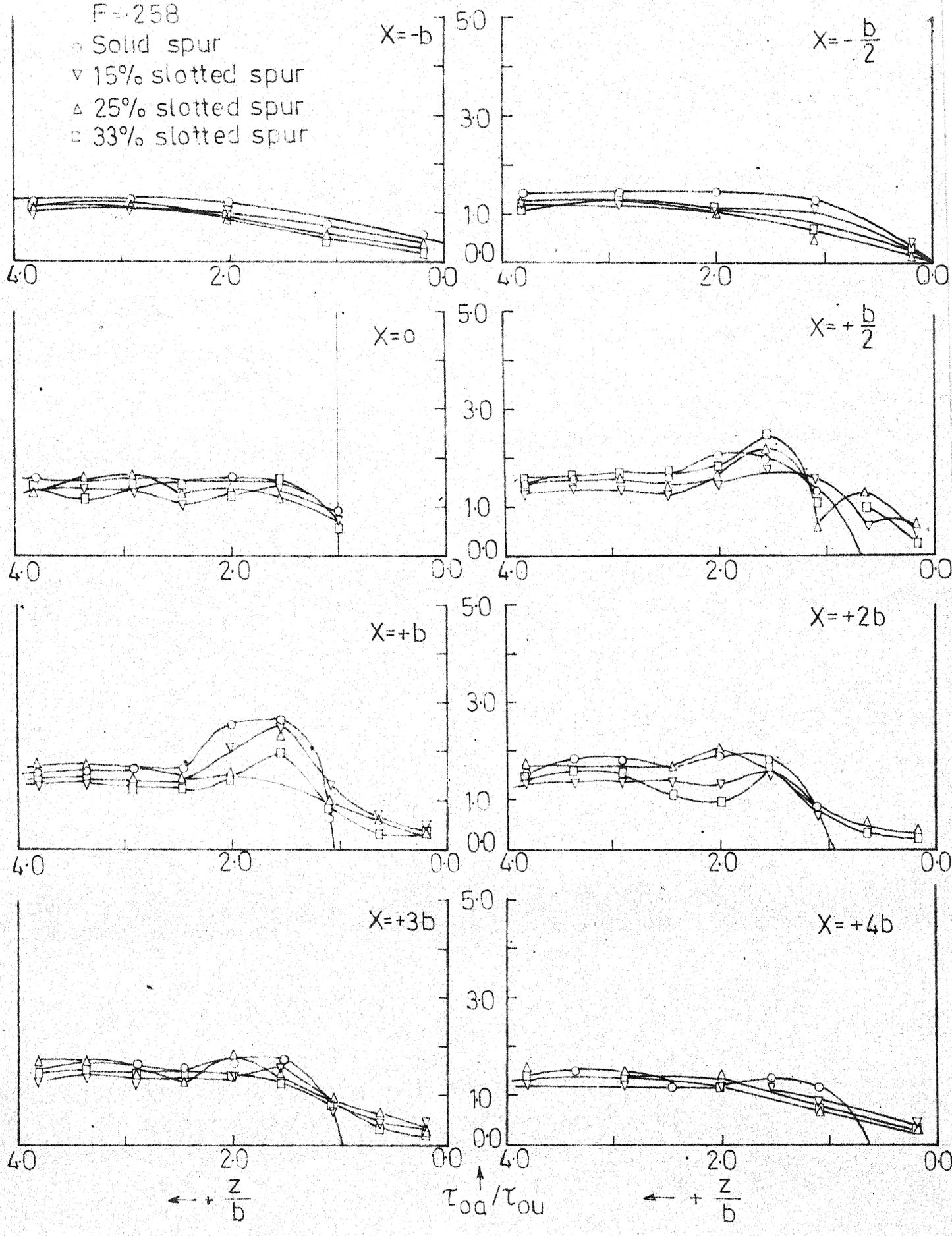

FIG·13 VARIATION OF BED SHEAR STRESS AT DIFFERENT FLOW CROSS SECTIONS

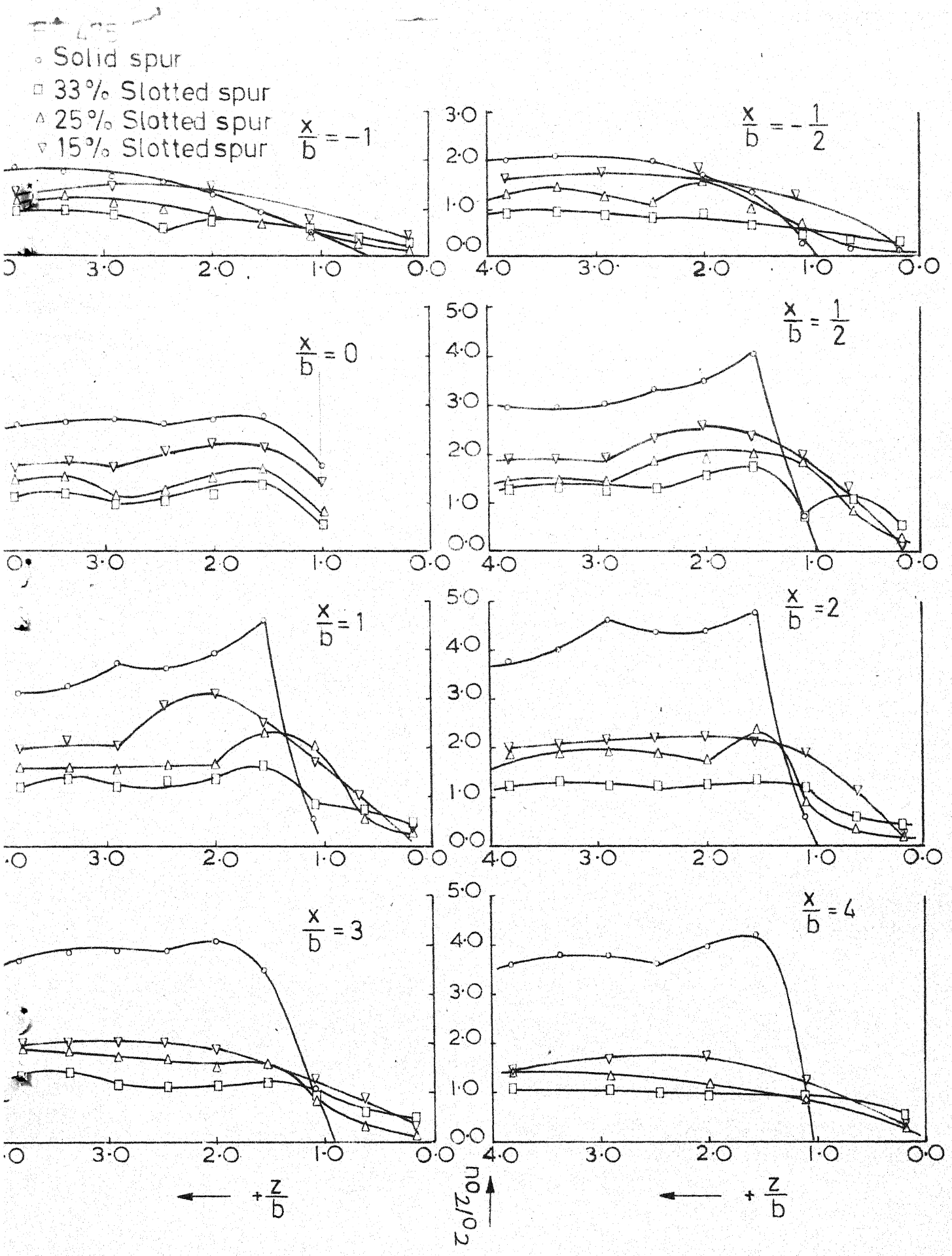

FIG.14 VARIATION OF BED SHEAR STRESS AT DIFFERENT FLOW CROSS SECTIONS

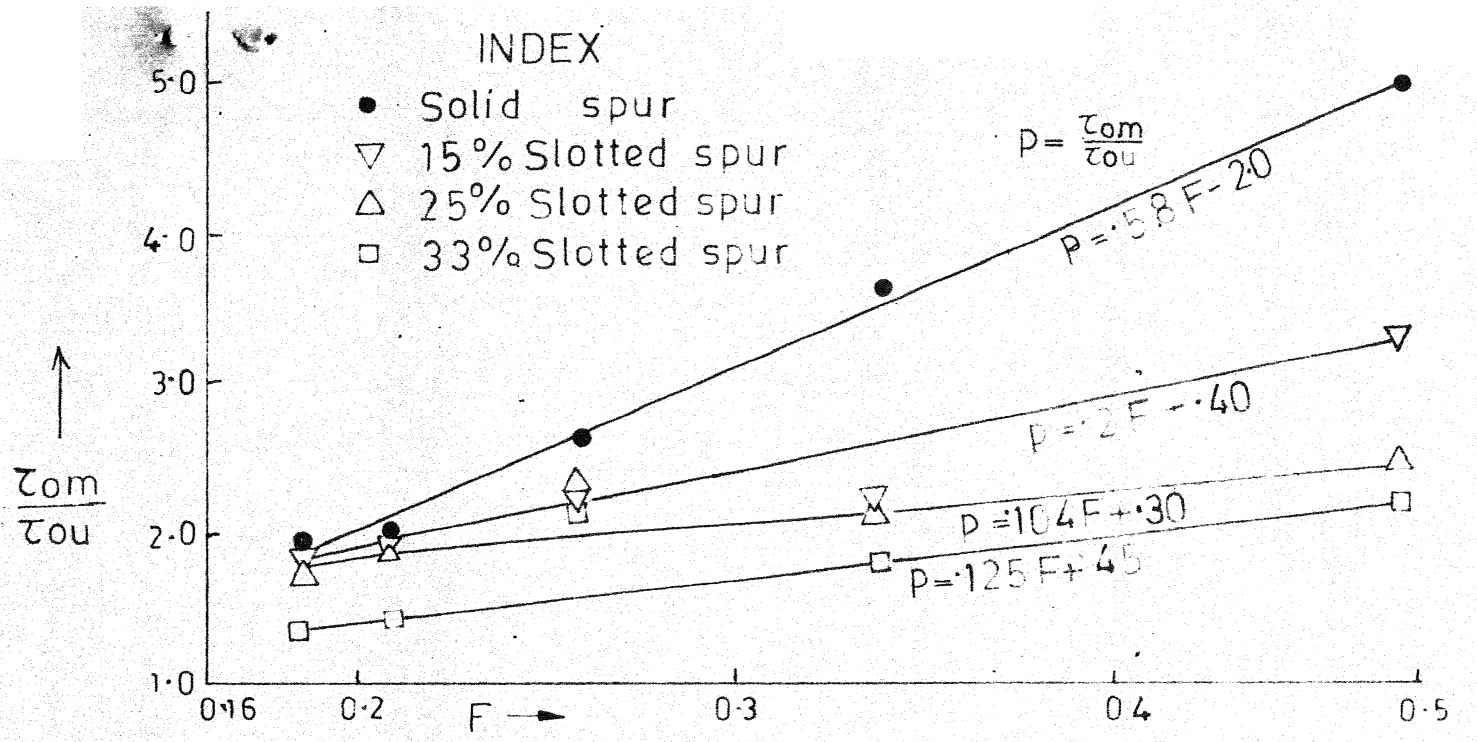

FIG.15 VARIATION OF MAXIMUM SHEAR STRESS WITH FROUDE NUMBER

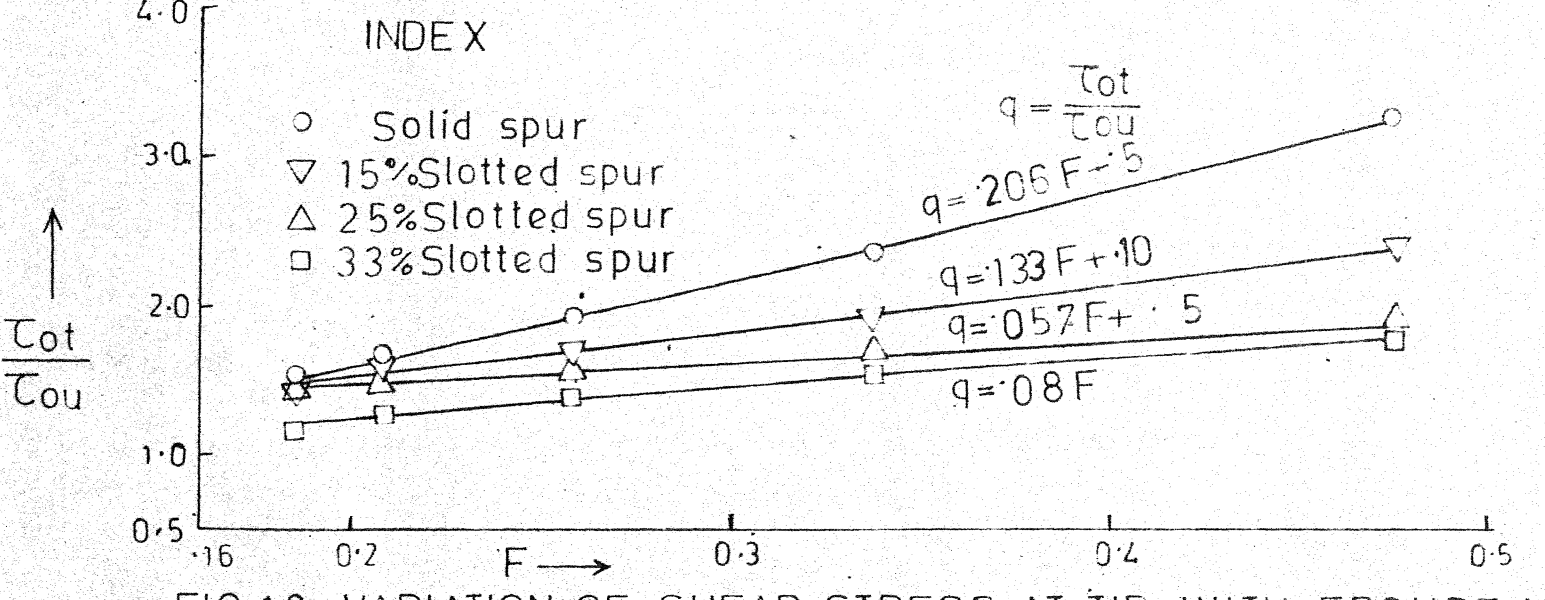

FIG.16 VARIATION OF SHEAR STRESS AT TIP WITH FROUDE NUMBER

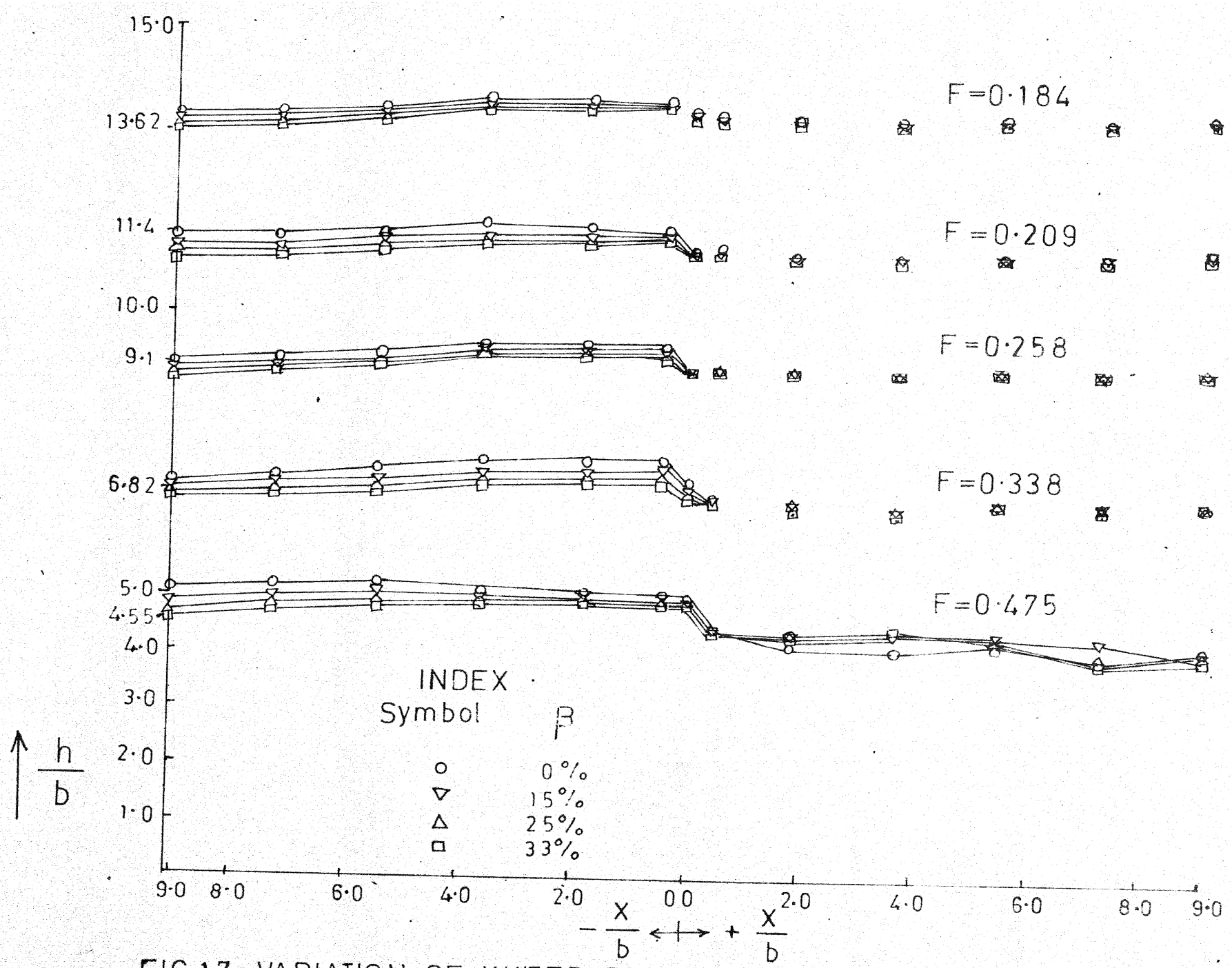

FIG.17 VARIATION OF WATER PROFILE ALONG THE FLOW DIRECTION

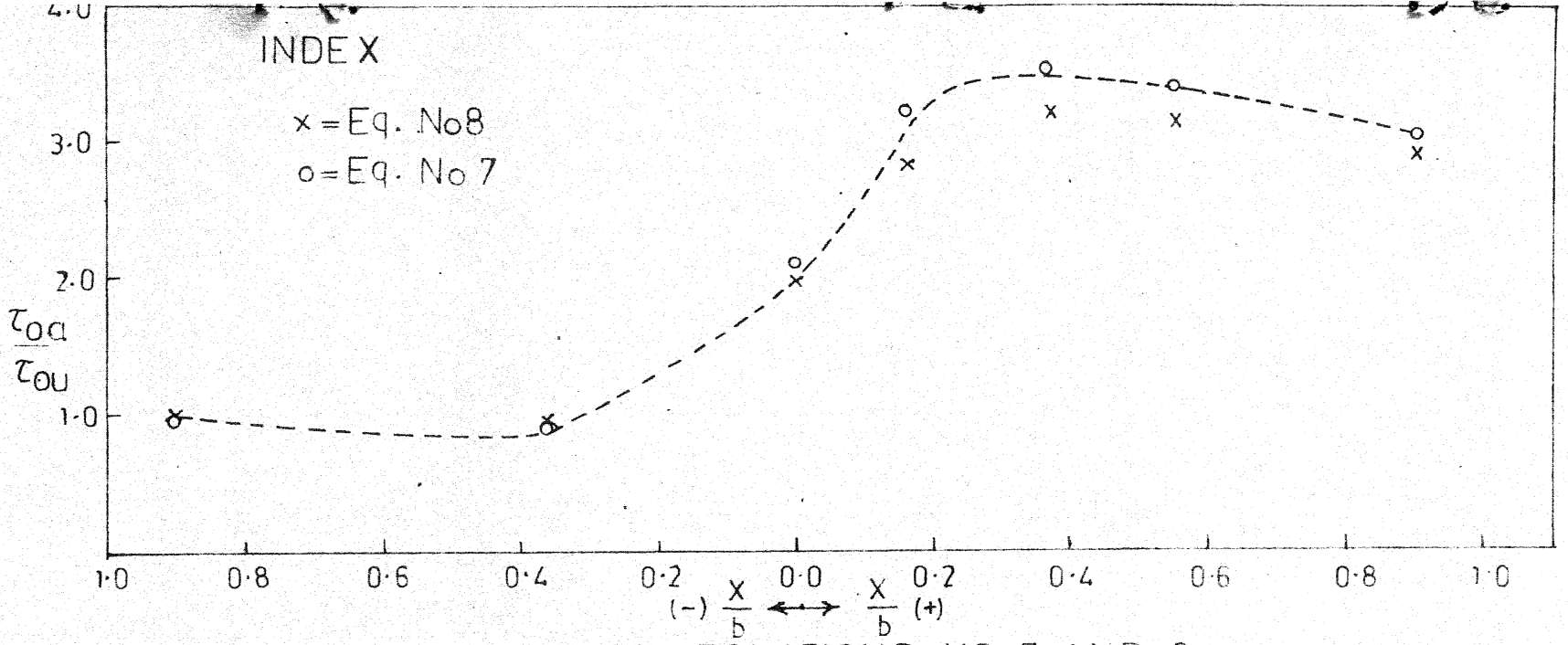

FIG.18. COMPARISION OF EQUATIONS NO. 7 AND 8

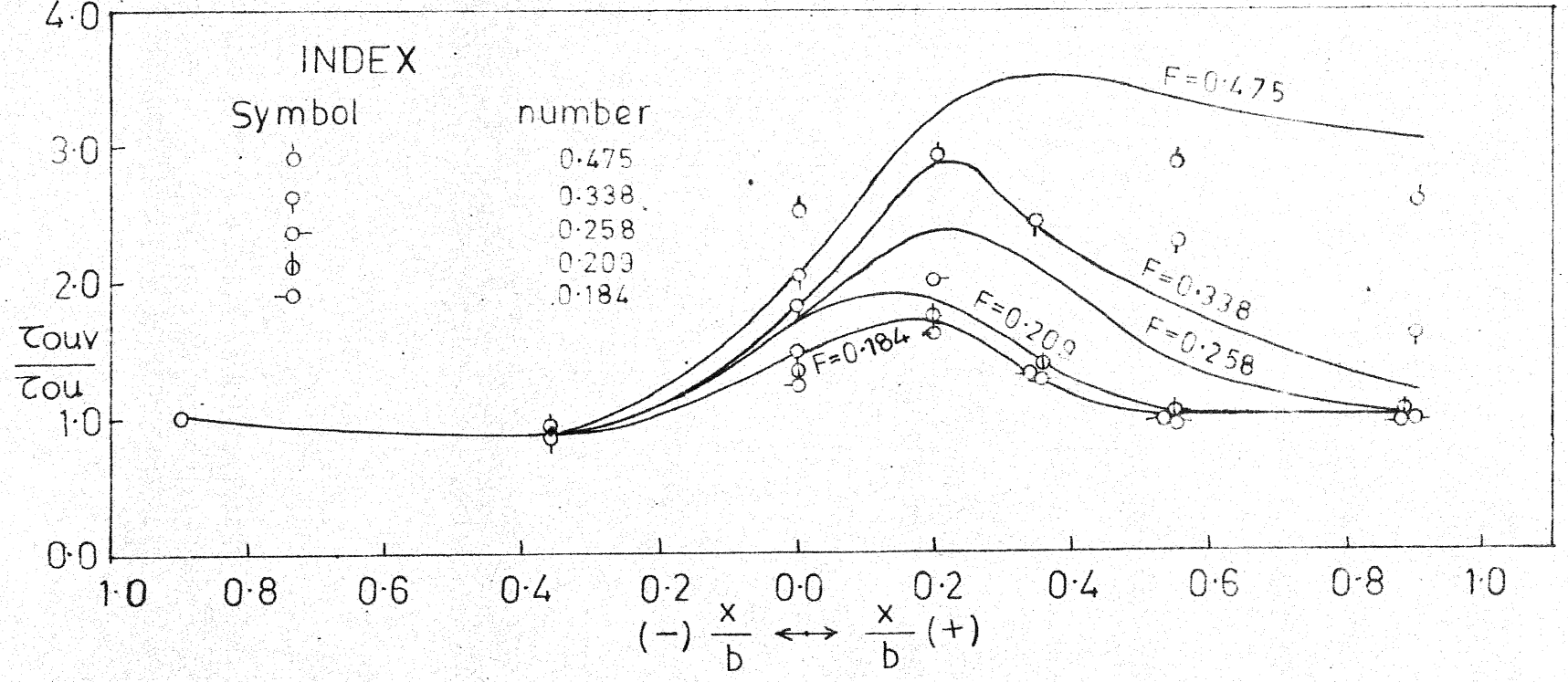

FIG.19. COMPARISION OF EQUATION 8 WITH EXPERIMENTAL OBSERVATION

F = ·475
V. POSITION: BOTTOM
H. SCALE : .2 sec/cm
V. SCALE : .5 volt/cm

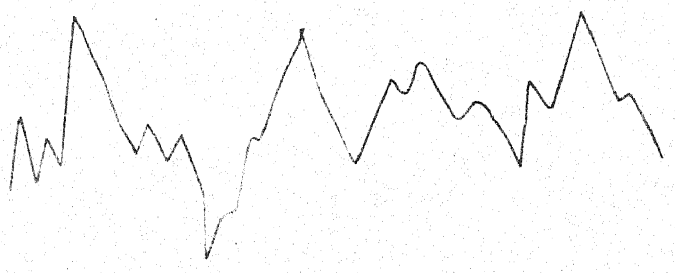

F = ·338
V. POSITION: BOTTOM
H. SCALE : .2sec/cm
V. SCALE: .5 volt/cm

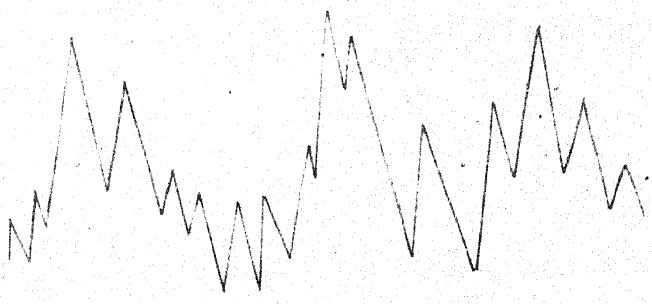

F = ·258
V. POSITION: 3cm from bottom
H. SCALE : .2 sec/cm
V. SCALE : ·5 volt/cm

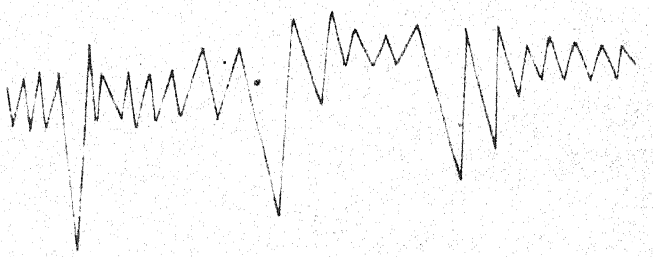

F = ·258
V. POSITION: 9 cm from bottom
H. SCALE : .1 sec/cm
V. SCALE : .1 volt/cm

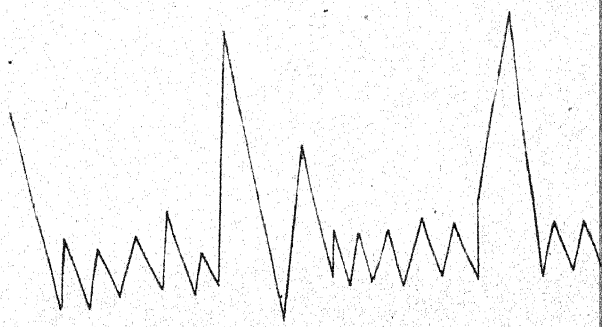

F = ·184
V. POSITION : 1 cm from bottom
H. SCALE : .1 sec/cm
V. SCALE : .5 volt/cm

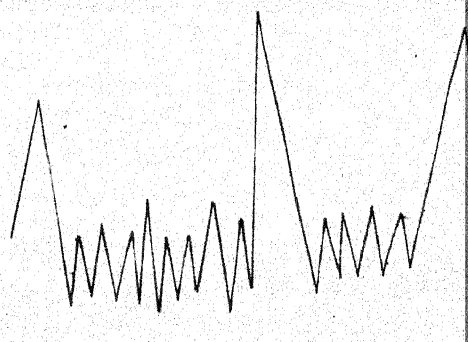

FIG·23 SCREEN DISPLAY OF VORTICES MEASUREMENTS FOR SOLID SPUR

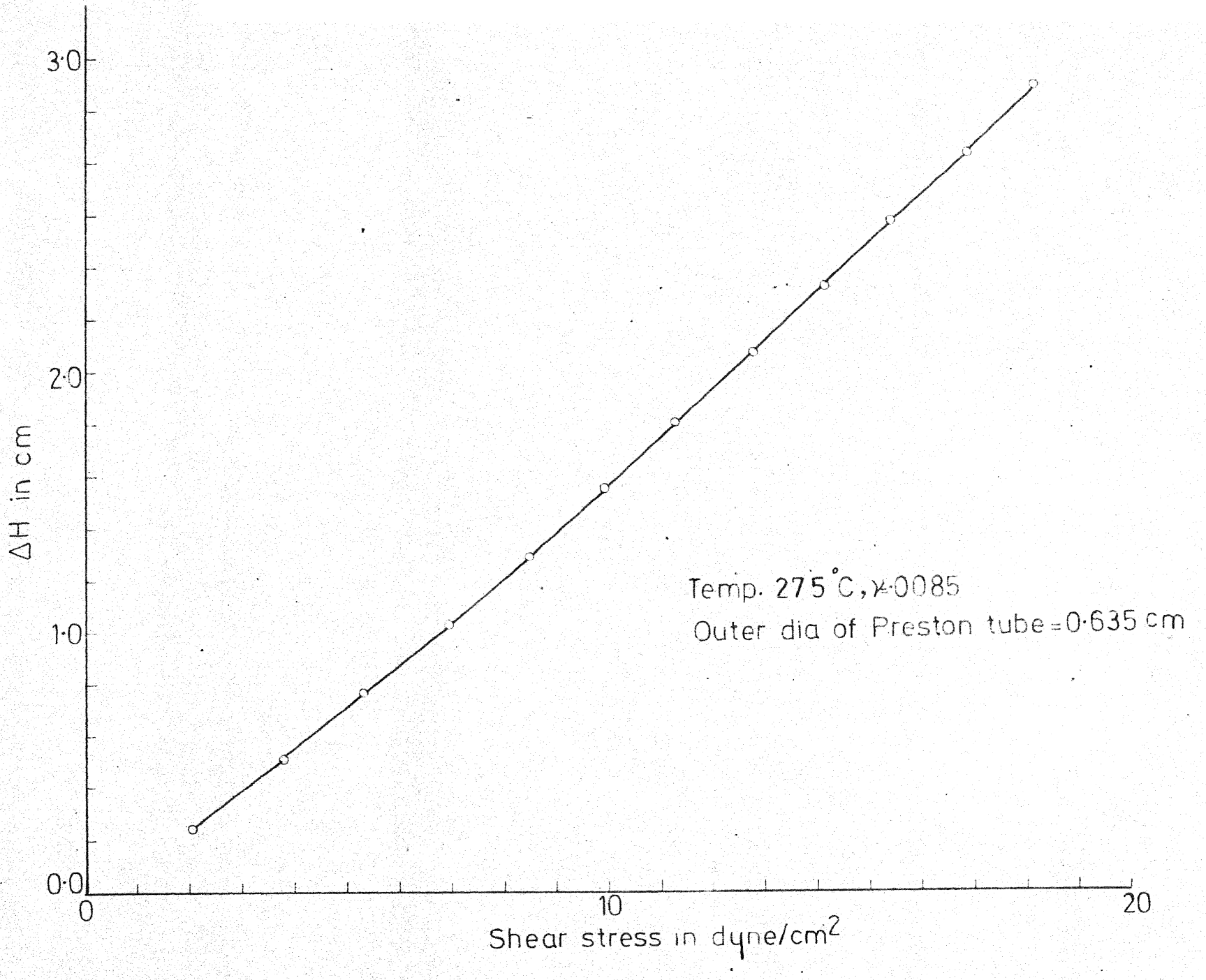

FIG·24 CALIBRATION CURVE FOR PRESTON TUBE